arXiv:cond-mat/0703091v1 [cond-mat.other] 3 Mar 2007

Ultracold Fermi gases in the BEC-BCS crossover: a review from the Innsbruck perspective

Rudolf Grimm

Institute of Experimental Physics and Center for Quantum Physics
University of Innsbruck, Technikerstraße 25, A-6020 Innsbruck, Austria

Institute for Quantum Optics and Quantum Information (IQOQI)
Austrian Academy of Sciences, Otto-Hittmair-Platz 1, A-6020 Innsbruck, Austria

1. – Introduction

By the time of the "Enrico Fermi" Summer School in June 2006, quantum degeneracy in ultracold Fermi gases has been reported by 13 groups worldwide [1, 2, 3, 4, 5, 6, 7, 8, 9, 10, 11, 12, 13]. The field is rapidly expanding similar to the situation of Bose-Einstein condensation at the time of the "Enrico Fermi" Summer School in 1998 [14]. The main two species for the creation of ultracold Fermi gases are the alkali atoms potassium (^{40}K) [1, 6, 8, 10, 11] and lithium (^{6}Li) [2, 3, 4, 5, 7, 9]. At the time of the School, degeneracy was reported for two new species, ^{3}He* [12] and ^{173}Yb [13], adding metastable and rare earth species to the list.

Fermionic particles represent the basic building blocks of matter, which connects the physics of interacting fermions to very fundamental questions. Fermions can pair up to form composite bosons. Therefore, the physics of bosons can be regarded as a special case of fermion physics, where pairs are tightly bound and the fermionic character of the constituents is no longer relevant. This simple argument already shows that the physics of fermions is in general much richer than the physics of bosons.

Systems of interacting fermions are found in many areas of physics, like in condensed-matter physics (e.g. superconductors), in atomic nuclei (protons and neutrons), in primordial matter (quark-gluon plasma), and in astrophysics (white dwarfs and neutron

© Società Italiana di Fisica

stars). Strongly interacting fermions pose great challenges for many-body quantum theories. With the advent of ultracold Fermi gases with tunable interactions and controllable confinement, unique model systems have now become experimentally available to study the rich physics of fermions.

In this contribution, we will review a series of experiments on ultracold, strongly interacting Fermi gases of ^{6}Li which we conducted at the University of Innsbruck. We will put our experiments into context with related work and discuss them according to the present state-of-the art knowledge in the field. After giving a brief overview of experiments on strongly interacting Fermi gases (Sec. **2**), we will discuss the basic interaction properties of ^{6}Li near a Feshbach resonance (Sec. **3**). Then we will discuss the main experimental results on the formation and Bose-Einstein condensation of weakly bound molecules (Sec. **4**), the crossover from a molecular Bose-Einstein condensate to a fermionic superfluid (Sec. **5**), and detailed studies on the crossover by collective modes (Sec. **6**) and pairing-gap spectroscopy (Sec. **7**).

2. – Brief history of experiments on strongly interacting Fermi gases

To set the stage for a more detailed presentation of our results, let us start with a brief general overview of the main experimental developments in the field of ultracold, strongly interacting Fermi gases; see also the contributions by D. Jin and W. Ketterle in these proceedings. The strongly interacting regime is realized when the scattering length, characterizing the two-body interacting strength, is tuned to large values by means of Feshbach resonances [15, 16]. In the case of Bose gases with large scattering lengths rapid three-body decay [17, 18, 19] prevents the experiments to reach the strongly interacting regime (1). Experiments with ultracold Fermi gases thus opened up a door to the new, exciting regime of many-body physics with ultracold gases.

The creation of a strongly interacting Fermi gas was first reported in 2002 by the group at Duke University [21]. They studied the expansion of a ^{6}Li gas with resonant interactions after release from the trap and observed hydrodynamic behavior. In similar experiments, the group at the ENS Paris provided measurements of the interaction energy of ultracold ^{6}Li in the strongly interacting region [22].

In 2003 ultracold diatomic molecules entered the stage. Their formation is of particular importance in atomic Fermi gases, as their bosonic nature is connected with a fundamental change of the quantum statistics of the gas. The JILA group demonstrated molecule formation in an ultracold Fermi gas of ^{40}K [23], followed by three groups working with ^{6}Li: Rice University [24], the ENS Paris [25], and Innsbruck University [26]. The latter experiments on ^{6}Li also demonstrated an amazing fact. Molecules made of fermionic atoms can be remarkably stable against inelastic decay, allowing for the formation of stable molecular quantum gases.

---

(1) This statement refers to macroscopically trapped gases of a large number of atoms. Highly correlated systems of bosons can be created in optical lattices [20].

In late 2003 three groups reported on the achievement of molecular Bose-Einstein condensation, our group (^{6}Li) [7], the JILA group (^{40}K) [27], and the MIT group (^{6}Li) [28], followed early in 2004 by the ENS group (^{6}Li) [29]. Early in 2004, the JILA group [30] and the MIT group [31] demonstrated pair condensation in strongly interacting Fermi gases with resonant interactions, i.e. beyond the BEC regime. These experiments demonstrated a new macroscopic quantum state of ultracold matter beyond well-established BEC physics, which has stimulated an enormous interest in the field.

The experiments then started to explore the crossover from a BEC-type system to a fermionic superfluid with Bardeen-Cooper-Schrieffer (BCS) type pairing. Elementary properties of the Fermi gas in the BEC-BCS crossover were studied by several groups. In Innsbruck, we showed that the crossover proceeds smoothly and can be experimentally realized in an adiabatic and reversible way [32]. At the ENS the crossover was investigated in the free expansion of the gas after release from the trap. Measurements of collective excitation modes at Duke University and in Innsbruck showed exciting observations and provided pieces of evidence for superfluidity in the strongly interacting gas. The Duke group measured very low damping rates, which could not be explained without invoking superfluidity [33]. Our work on collective oscillations [34] showed a striking breakdown of the hydrodynamic behavior of the gas when the interaction strength was changed, suggesting a superfluid-normal transition.

Spectroscopy on fermionic pairing based on a radio-frequency method showed the “pairing gap” of the strongly interacting gas along the BEC-BCS crossover [35]. In these experiments performed in Innsbruck, temperature-dependent spectra suggested that the resonantly interacting Fermi gas was cooled down deep into the superfluid regime. A molecular probe technique of pairing developed at Rice University provided clear evidence for pairing extending through the whole crossover into the weakly interacting BCS regime [36]. Measurements of the heat capacity of the strongly interacting gas performed at Duke University showed a transition at a temperature where superfluidity was expected [37]. After several pieces of experimental evidence provided by different groups, the final proof of superfluidity in strongly interacting Fermi gases was given by the MIT group in 2005 [38]. They observed vortices and vortex arrays in a strongly interacting Fermi gas in various interaction regimes.

New phenomena were recently explored in studies on imbalanced spin-mixtures at Rice University [39] and at MIT [40]. These experiments have approached a new frontier, as such systems may offer access to novel superfluid phases. Experiments with imbalanced spin-mixtures also revealed the superfluid phase transition in spatial profiles of the ultracold cloud [41].

3. – Interactions in a ^{6}Li spin mixture

Controllable interactions play a crucial role in all experiments on strongly interacting Fermi gases. To exploit an *s*-wave interaction at ultralow temperatures, non-identical particles are needed; thus the experiments are performed on mixtures of two different spin states. Feshbach resonances [15, 16, 42] allow tuning the interactions through vari-

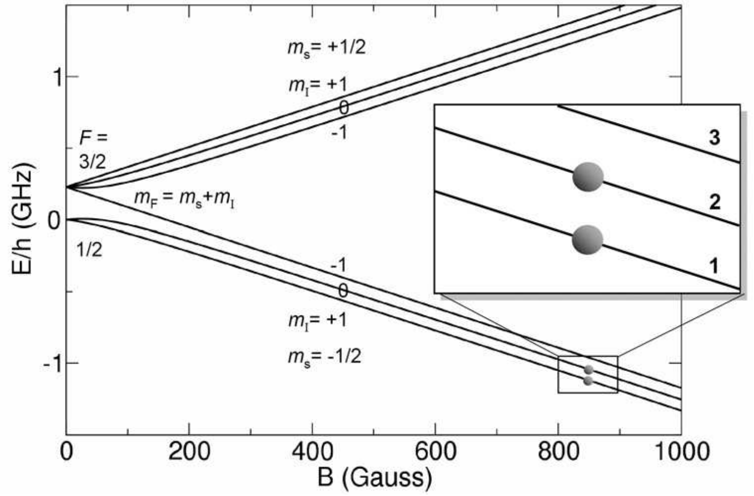

Fig. 1. – Energy levels for the electronic ground state of ^{6}Li atoms in a magnetic field. The experiments on strongly interacting Fermi gases are performed in the high magnetic field range, where the nuclear spin essentially decouples from the electron spin. The two-component atomic mixture is created in the lowest two states, labelled with 1 and 2 (inset), close to the broad Feshbach resonance centered at 834 G.

ations of an external magnetic field. In this section, we review the two-body interaction properties of ^{6}Li. In particular, we discuss the behavior close to a wide Feshbach resonance with very favorable properties for interaction tuning in strongly interacting Fermi gases.

3˙1. *Energy levels of* ^{6}*Li atoms in a magnetic field.* – The magnetic-field dependence of the energy structure of ^{6}Li atoms in the electronic $\mathrm{S}_{1/2}$ ground state is shown in Fig. 1. The general behavior is similar to any alkali atom [43] and is described by the well-known Breit-Rabi formula. At zero magnetic field, the coupling of the ^{6}Li nuclear spin ($I = 1$) to the angular momentum of the electron ($J = 1/2$) leads to the hyperfine splitting of 228.2 MHz between the states with quantum numbers $F = I + J$ and $F = I - J$.

Already at quite moderate magnetic fields the Zeeman effect turns over into the high-field regime, where the Zeeman energy becomes larger than the energy of the hyperfine interaction. Here the nuclear spin essentially decouples from the electron spin. In atomic physics this effect is well known as the "Paschen-Back effect of the hyperfine structure" or "Back-Goudsmit effect" [43]. In the high-field region the states form two triplets, depending on the orientation of the electron spin ($m_s = \pm 1/2$), where the states are characterized by the orientation of the nuclear spin with quantum number m_I. For simplicity, we label the states with numbers according to increasing energy (see inset in Fig. 1). The lowest two states 1 and 2 are of particular interest for creating stable spin mixtures. These two states $m_s = -1/2, m_I = +1$ ($m_s = -1/2, m_I = 0$) are adiabatically

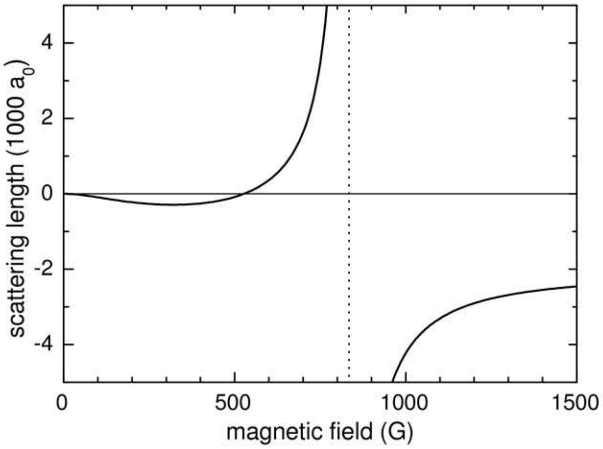

Fig. 2. – Tunability of the s-wave interactions in a spin mixture of ^{6}Li atoms in the two lowest spin states 1 and 2. The s-wave scattering length a shows a pronounced, broad resonance as a function of the magnetic field [44, 45]. The vertical dotted line indicates the exact resonance field (834 G) where a goes to infinity and the interaction is only limited through unitarity.

connected with the states $F = 1/2, m_F = 1/2$ $(F = 1/2, m_F = -1/2)$ at low magnetic fields.

3˙2. *Tunability at the marvelous 834 G Feshbach resonance.* – Interactions between ^{6}Li atoms in states 1 and 2 show a pronounced resonance in s-wave scattering [44, 45] with favorable properties for the experiments on strongly interacting Fermi gases. Fig. 2 displays the scattering length a as a function of the magnetic field B. The center of the resonance, i.e. the point where a diverges, is located at 834 G. This resonance center is of great importance to realize the particularly interesting situation of a universal Fermi gas in the unitarity limit; see discussion in **5**˙3.

The investigation of the broad Feshbach resonance in ^{6}Li has a history of almost ten years. In 1997, photoassociation spectroscopy performed at Rice University revealed a triplet scattering length that is negative and very large [46]. A theoretical collaboration between Rice and the Univ. of Utrecht [44] then led to the prediction of the resonance near 800 G. In 2002, first experimental evidence for the resonance was found at MIT [47], at Duke University [48], and in Innsbruck [49]. At about 530 G, experiments at Duke and in Innsbruck showed the zero crossing of the scattering length that is associated with the broad resonance. The MIT group observed an inelastic decay feature in a broad magnetic-field region around 680 G. The decay feature was also observed at the ENS Paris, but at higher fields around 720 G [22]. The ENS group also reported indications of the resonance position being close to 800 G. In Innsbruck the decay feature was found [50] in a broad region around 640 G (2). Molecule dissociation experiments at MIT [31, 51] provided a lower bound of 822 G for the resonance point. To date the most accurate knowledge on $a(B)$ in ^{6}Li spin mixtures results from an experiment-theory collaboration between Innsbruck and NIST on radio-frequency spectroscopy on weakly bound molecules [45]. This work puts the resonance point to 834.1 G within an uncertainty of ± 1.5 G.

The dependence $a(B)$ near the Feshbach resonance can be conveniently described by a fit formula [45], which approximates the scattering length in a range between 600 and 1200 G to better than 99%,

$$a(B) = a_{\mathrm{bg}} \left(1 + \frac{\Delta B}{B - B_0} \right) (1 + \alpha (B - B_0)) \tag{1}$$

with $a_{\mathrm{bg}} = -1405\, a_0$, $B_0 = 834.15\,\mathrm{G}$, $\Delta B = 300\,\mathrm{G}$, and $\alpha = 0.040\,\mathrm{kG}^{-1}$; here $a_0 = 0.529177\,\mathrm{nm}$ is Bohr's radius.

Concerning further Feshbach resonances in ^{6}Li, we note that besides the broad 834 G resonance in the $(1,2)$ spin mixture, similar broad s-wave resonances are found in $(1,3)$ and in $(2,3)$ mixtures with resonance centers at 690 G and at 811 G, respectively [45]. The $(1,2)$ spin mixture also features a narrow Feshbach resonance near 543 G with a width of roughly 100 mG [24, 51]. Moreover, Feshbach resonances in p-wave scattering of ^{6}Li have been observed in $(1,1)$, $(1,2)$, and $(2,2)$ collisions at the ENS [52] and at MIT [51].

3˙3. *Weakly bound dimers.* – A regime of particular interest is realized when the scattering length a is very large and positive. The scale for "very large" is set by the van der Waals interaction between two ^{6}Li atoms, characterized by a length $R_{\mathrm{vdW}} = (mC_6/\hbar^2)^{1/4}/2 = 31.26\, a_0$ (for ^{6}Li, $C_6 = 1393$ a.u. and the atomic mass is $m = 6.015$ u). For $a \gg R_{\mathrm{vdW}}$, a weakly bound molecular state exists with a binding energy given by the universal formula (3)

$$E_{\mathrm{b}} = \frac{\hbar^2}{ma^2}. \tag{2}$$

In this regime, the molecular wave function extends over a much larger range than the interaction potential and, for large interatomic distances $r \gg R_{\mathrm{vdW}}$, falls off exponentially as $\exp(-r/a)$. The regime, in which a bound quantum object is much larger than a

---

(2) The interpretation of these inelastic decay features involves different processes, which depend on the particular experimental conditions, see also **4**˙3. In a three-body recombination event, immediate loss occurs when the release of molecular binding energy ejects the particles out of the trap. Another mechanism of loss is vibrational quenching of trapped, weakly bound molecules. The fact that, in contrast to bosonic quantum gases, maximum inelastic decay loss does not occur at the resonance point, but somewhere in the region of positive scattering length is crucial for the stability of strongly interacting Fermi gases with resonant interactions.

(3) A useful correction to the universal expression for the non-zero range of the van der Waals potential is $E_{\mathrm{b}} = \hbar^2/(m(a - \bar{a})^2)$ where $\bar{a} = 0.956\, R_{\mathrm{vdW}}$ [53].

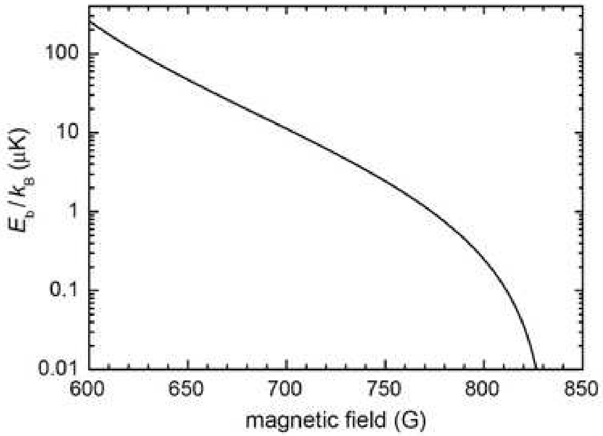

Fig. 3. – Binding energy E_b of weakly bound ^{6}Li molecules, which exist on the lower side of the 834 G Feshbach resonance. Here we use temperature units ($k_\mathrm{B} \times 1\,\mu\mathrm{K} \approx h \times 20.8\,\mathrm{kHz}$) for a convenient comparison with our experimental conditions.

classical system, is also referred to as the "quantum halo regime" [54]. For quantum halo states, the details of the short-range interaction are no longer relevant and the physics acquires universal character [55]. Here two-body interactions are completely characterized by a as a single parameter.

From these considerations, we understand that the lower side of the 834 G Feshbach resonance in ^{6}Li is associated with the regime of weakly bound (quantum halo) molecules. The binding energy of the weakly bound ^{6}Li molecular state is plotted in Fig. 3 as a function of the magnetic field.

Weakly bound molecules made of *fermionic* atoms exhibit striking scattering properties [56]. As a big surprise, which enormously boosted the field of ultracold fermions in 2003, these dimers turned out to be highly stable against inelastic decay in atom-dimer and dimer-dimer collisions. The reason for this stunning behavior is a Pauli suppression effect. The collisional quenching of a weakly bound dimer to a lower bound state requires a close encounter of three particles. As this necessarily involves a pair of identical fermions the process is Pauli blocked. The resulting collisional stability is in sharp contrast to weakly bound dimers made of bosonic atoms [57, 58, 59, 60], which are very sensitive to inelastic decay. The amazing properties of weakly bound dimers made of fermions were first described in Ref. [56]. Here we just summarize the main findings, referring the reader to the lecture of G. Shlyapnikov in these proceedings for more details.

For elastic atom-dimer and dimer-dimer collisions, Petrov et al. [56] calculated the scattering lengths

$$a_\mathrm{ad} = 1.2\,a, \tag{3}$$

$$a_\mathrm{dd} = 0.6\,a, \tag{4}$$

respectively. Inelastic processes, described by the loss-rate coefficients $\alpha_{\rm ad}$ and $\alpha_{\rm dd}$, follow the general scaling behavior [56]

$$\alpha_{\rm ad} = c_{\rm ad}\frac{\hbar R_{\rm vdW}}{m}\left(\frac{R_{\rm vdW}}{a}\right)^{3.33}, \tag{5}$$

$$\alpha_{\rm dd} = c_{\rm dd}\frac{\hbar R_{\rm vdW}}{m}\left(\frac{R_{\rm vdW}}{a}\right)^{2.55}. \tag{6}$$

Here the dimensionless coefficients $c_{\rm ad}$ and $c_{\rm dd}$ depend on non-universal short-range physics. We point out that, for typical experimental conditions in molecular BEC experiments (see Sec. **4**), the factor $(R_{\rm vdW}/a)^{2.55}$ results in a gigantic suppression of five orders of magnitude in inelastic dimer-dimer collisions!

The general scaling behavior of inelastic loss is universal and should be the same for ^{6}Li and ^{40}K, consistent with measurements on both species [25, 26, 61] The pre-factors $C_{\rm ad}$ and $C_{\rm dd}$, however, are non-universal as they depend on short-range three-body physics. A comparison of the experiments on both species shows that inelastic decay of weakly bound molecules is typically two orders of magnitude faster for ^{40}K than for ^{6}Li. This difference can be attributed to the larger van der Waals length of ^{40}K in combination with its less favorable short-range interactions.

This important difference in inelastic decay is the main reason why experiments on ^{6}Li and ^{40}K follow different strategies for the creation of degenerate Fermi gases. In ^{6}Li, the regime of weakly bound dimers on the molecular side of the Feshbach resonance opens up a unique route into deep degeneracy, as we will discuss in the following Section.

4. – The molecular route into Fermi degeneracy: creation of a molecular Bose-Einstein condensate

In experiments on ^{6}Li gases, a molecular Bose-Einstein condensate (mBEC) can serve as an excellent starting point for the creation of strongly interacting Fermi gases in the BEC-BCS crossover regime. In this section, after discussing the various approaches followed by different groups, we describe the strategy that we follow in Innsbruck to create the mBEC.

4˙1. *A brief review of different approaches.* – The experiments on strongly interacting gases of ^{6}Li in different laboratories (in alphabetical order: Duke University, ENS Paris, Innsbruck University, MIT, Rice University) are based on somewhat different approaches. The first and the final stages of all experiments are essentially the same. In the first stage, standard laser cooling techniques [62] are applied to decelerate the atoms in an atomic beam and to accumulate them in a magneto-optic trap (MOT); for a description of our particular setup see Refs. [63, 50]. In the final stage, far-detuned optical dipole traps [64] are used to store and manipulate the strongly interacting spin mixture. The creation of such a mixture requires trapping in the high-field seeking spin states 1 and 2 (see Fig. 1), which cannot be achieved magnetically. The main differences in the experimental approaches pursued in the five laboratories concern the intermediate stages of trapping and cooling. The general problem is to achieve an efficient loading of many ^{6}Li atoms into the small volume of a far-detuned optical dipole trap.

At Rice Univ., ENS, and MIT, magnetic traps are used as an intermediate stage [2, 3, 5]. This approach offers the advantage of a large volume and efficient transfer from a MOT with minimum loading losses. To achieve efficient cooling in the magnetic trap, the experiments then use bosonic atoms as a cooling agent. At Rice Univ. and at ENS, the ^{6}Li atoms are trapped together with the bosonic isotope ^{7}Li [2, 3]. The isotope mixture can be efficiently cooled to degeneracy by radio-frequency induced evaporation. Finally the sample is loaded into an optical dipole trap, and the atoms are transferred from their magnetically trappable, low-field seeking spin state into the high-field seeking states 1 and 2. The internal transfer is achieved through microwave and radio-frequency transitions. In this process it is important to create an incoherent spin mixture, which requires deliberate decoherence in the sample. At MIT the approach is basically similar [5], but a huge BEC of Na atoms is used as the cooling agent. This results in an exceptionally large number of atoms in the degenerate Fermi gas [65]. In all three groups (Rice, ENS, MIT), final evaporative cooling is performed on the strongly interacting spin mixture by reducing the power of the optical trap.

The experiments at Duke University [21] and in Innsbruck [7] proceed in an all-optical way without any intermediate magnetic traps. To facilitate direct loading from the MOT, the optical dipole traps used in these experiments have to start with initially very high laser power. For the final stage of the evaporation much weaker traps are needed. Therefore, the all-optical approach in general requires a large dynamical range in the optical trapping power. The Duke group uses a powerful 100-W CO_2 laser source [4] both for evaporative cooling and for the final experiments. In Innsbruck we employ two different optical trapping stages to optimize the different phases of the experiment.

4˙2. *The all-optical Innsbruck approach.* – An efficient transfer of magneto-optically trapped lithium atoms into an optical dipole trap is generally much more difficult than for the heavy alkali atoms. The much higher temperatures of lithium in a MOT of typically a few hundred microkelvin [63] require deep traps with a potential depth of the order of 1 mK. We overcome this bottleneck of dipole trap loading by means of a deep large-volume dipole trap serving as a “funnel”. The trap is realized inside a build-up cavity constructed around the glass cell [70]. The linear resonator enhances the power of a 2-W infrared laser (Nd:YAG at a wavelength of 1064 nm) by a factor of ∼150 and, with a Gaussian beam waist of 160μm, allows us to create a 1 mK deep optical standing-wave trapping potential. Almost 10^7 atoms in the lower hyperfine level with $F = 1/2$ can be loaded from the ^{6}Li MOT into the resonator-enhanced dipole trap at a temperature of typically a few 100 μK. Note that, when loaded from the MOT, the spin mixture of states 1 and 2 in the optical dipole trap is incoherent from the very beginning.

Then we apply a single beam from a 10-W near-infrared laser (wavelength 1030 nm), which is focussed to a waist of typically a few ten μm (∼25 μm in our earlier experiments [7, 32, 34], ∼50μm in more recent work [71]), overlapping it with the atom cloud in the

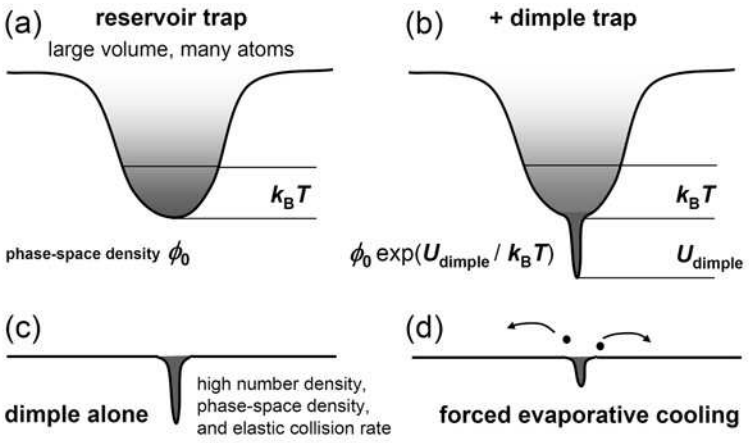

Fig. 4. – Illustration of the "dimple trick". The atoms are first transferred from the MOT into a large-volume optical reservoir trap (a), here implemented inside of an optical resonator. A narrow "dimple" potential (b) is then added and thermalization leads to a huge increase of the local density and phase-space density according to the Boltzmann factor as the temperature is set by the reservoir. After removal of the reservoir trap (c) one obtains a very dense sample optically trapped sample. Forced evaporative cooling can then be implemented (d) by ramping down the trap power. The dimple trick, originating from work in Refs. [66] and [67], has proven a very powerful tool for the all-optical creation of degenerate quantum gases [68, 69].

standing-wave trapping potential. The total optical potential can then be regarded as a combination of a large-volume "reservoir" trap in combination with a narrow "dimple" potential. The dimple is efficiently filled through elastic collisions resulting in a large increase in local density, phase-space density, and elastic collisions rate; this "dimple trick" is illustrated in Fig. 4. After removal of the reservoir, i.e. turning off the standing-wave trap, we obtain a very dense cloud of $\sim 1.5 \times 10^6$ atoms at a temperature $T \approx 80\,\mu$K, a peak density of $\sim 10^{14}\,\text{cm}^{-1}$, a peak phase-space density of 5×10^{-3}, and a very high elastic collision rate of $5 \times 10^4\,\text{s}^{-1}$. In this way, excellent starting conditions are realized for evaporative cooling.

A highly efficient evaporation process is then forced by ramping down the laser power by typically three orders of magnitude within a few seconds. The formation of weakly bound molecules turns out to play a very favorable role in this process and eventually leads to the formation of a molecular BEC. The details of this amazing process will be elucidated in the following.

4˙3. *Formation of weakly bound molecules.* – The formation of weakly bound molecules in a *chemical atom-molecule equilibrium* [72, 73] plays an essential role in the evaporative cooling process; see illustration in Fig. 5. In the ^{6}Li gas, molecules are formed through three-body recombination. As the molecular binding energy E_b is released into kinetic

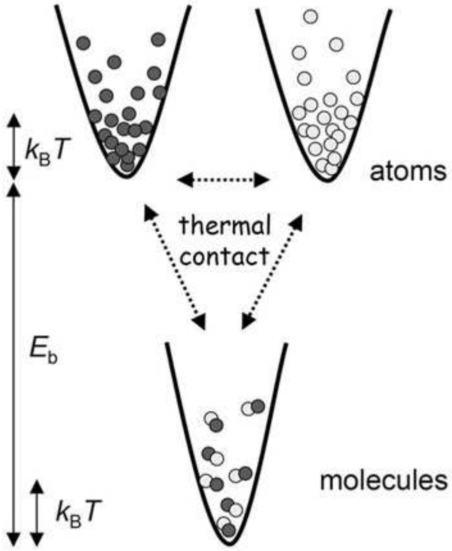

Fig. 5. – Illustration of the atom-molecule thermal equilibrium in a trapped ^{6}Li gas at the molecular side of the Feshbach resonance. Atoms in the two spin states and molecules represent three sub-ensembles in thermal contact (thermal energy $k_\mathrm{B}T$). The molecules are energetically favored because of the binding energy E_b, which is reflected in the Boltzmann factor in Eq. 7. The equilibrium can also be understood in terms of a balance of the chemical processes of exoergic recombination and endoergic dissociation [72].

energy, this process is exoergic and thus leads to heating of the sample (^{4}). The inverse chemical process is dissociation of molecules through atom-dimer and dimer-dimer collisions. These two-body processes are endoergic and can only happen when the kinetic energy of the collision partners is sufficient to break up the molecular bond. From a balance of recombination (exoergic three-body process) and dissociation (endoergic two-body processes) one can intuitively understand that molecule formation is favored at low temperatures and high number densities, i.e. at high phase-space densities.

For a non-degenerate gas, the atom-molecule equilibrium follows a simple relation [72]

$$\phi_\mathrm{mol} = \phi_\mathrm{at}^2 \exp\left(\frac{E_\mathrm{b}}{k_\mathrm{B}T}\right), \tag{7}$$

where ϕ_mol and ϕ_at denote the molecular and atomic phase-space densities, respectively.

(^{4}) The relation of released binding energy E_b to the trap depth is crucial whether the recombination products remain trapped and further participate in the thermalization processes. For low trap depth the recombination leads to immediate loss. This explains why the loss features observed by different groups [47, 22, 50] shift towards lower fields at higher trap depths.

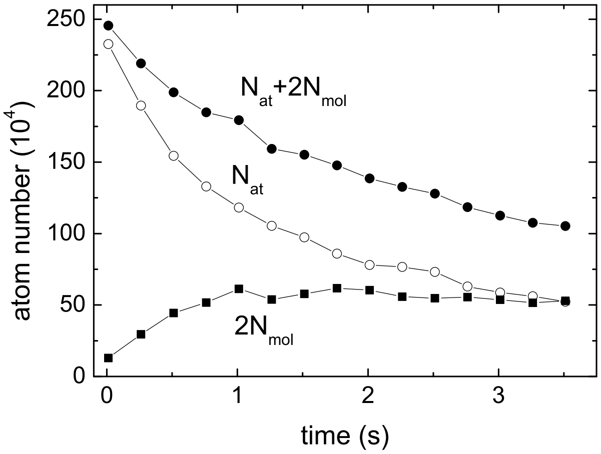

Fig. 6. – Experimental results [26] demonstrating how an ultracold ^{6}Li gas approaches a chemical atom-molecule equilibrium on the molecular side of the Feshbach resonance. The experiment starts with a non-degenerate, purely atomic gas at a temperature of $2.5\,\mu$K and a peak atomic phase-space density of 0.04. The magnetic field is set to 690 G, where $a = 1420\,a_0$ and $E_{\rm b}\,/k_{\rm B} = 15\,\mu$K. $N_{\rm at}$ and $N_{\rm mol}$ denote the number of unbound atoms and the number of molecules, respectively. The total number of unbound and bound atoms $2N_{\rm mol} + N_{\rm at}$ slowly decreases because of residual inelastic loss, see **3**˙3.

The Boltzmann factor enhances the fraction of molecules in a trapped sample and can (partially) compensate for a low atomic phase-space density. Including the effect of Fermi degeneracy, the thermal atom-molecule equilibrium was theoretically investigated in Ref. [73].

We have experimentally studied the thermal atom-molecule equilibrium in Ref. [26]. Fig. 6 illustrates how an initially pure atomic gas tends to an atom-molecule equilibrium. The experiment was performed at a magnetic field of 690 G and a temperature $T = 2.5\,\mu$K with a molecular binding energy of $E_{\rm b}/k_{\rm B} = 15\,\mu$K. The observation that more than 50% of the atoms tend to form molecules at a phase-space density of a factor of thirty from degeneracy, highlights the role of the Boltzmann factor (see Eq. 7) in the equilibrium. Note that in Fig. 6, the total number of particles decreases slowly because of residual inelastic decay of the molecules. The magnetic field of 690 G is too far away from resonance to obtain a full suppression of inelastic collisions. Further experiments in Ref. [26] also demonstrated how an atom-molecule thermal equilibrium is approached from an initially pure molecular sample. In this case atoms are produced through dissociation of molecules at small molecular binding energies closer to the Feshbach resonance.

An experiment at ENS [25] demonstrated the adiabatic conversion of a degenerate ^{6}Li Fermi gas produced at $a < 0$ into a molecular gas by slowly sweeping across the Feshbach resonance. This resulted in a large molecular fraction of up to 85% and experimental conditions close to mBEC. Before the work in ^{6}Li, molecule formation in an ultracold Fermi

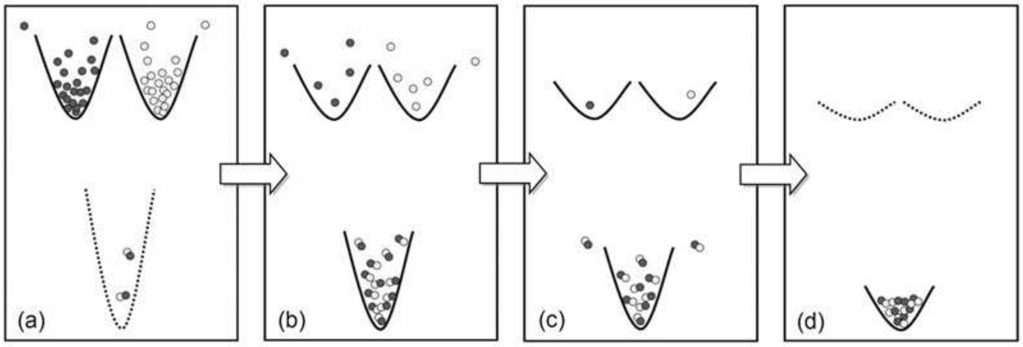

Fig. 7. – Stages of evaporative cooling on the molecular side of the Feshbach resonance. (a) For a hot gas, very few molecules are present and the evaporation can be understood in terms of elastic collisions in the atomic spin mixture. (b) As the gas gets colder the chemical atom-molecule equilibrium begins to favor the molecules. (c) Further evaporation removes atoms but not molecules because of the two times different trap depths. (d) After disappearance of the atoms, evaporation can be fully understood in terms of the molecular gas. This eventually leads to molecular Bose-Einstein condensation.

gas through a Feshbach sweep was demonstrated with ^{40}K at JILA [23]. The long-lived nature of the ^{40}K molecules close to the Feshbach resonance was demonstrated in later work [61]. Note that long-lived molecules of ^{6}Li were also produced from a degenerate gas at Rice Univ. [24]. This experiment, however, was performed by sweeping across the narrow Feshbach resonance at 543 G. The observed stability cannot be explained in terms of the Pauli suppression arguments in Sec. **3**˙3 and, to the best knowledge of the author, still awaits a full interpretation.

4˙4. *Evaporative cooling of an atom-molecule mixture.* – Based on the thermal atom-molecule equilibrium arguments discussed before, we can now understand why the evaporation process works so well on the molecular side of the Feshbach resonance.

Experimentally, we found that highly efficient evaporative cooling can be performed at a fixed magnetic field around 764 G [7]. At this optimum field, the large scattering length $a = +4500\,a_0$ warrants a large stability of the molecules against inelastic decay (see **3**˙3). The corresponding binding energy $E_\mathrm{b}/k_\mathrm{B} = 1.5\,\mu$K is small enough to minimize recombination heating during the cooling process. However, it is larger than the typical Fermi energies in the final evaporation stage of a few hundred nK, which favors the molecule formation in the last stage of the cooling process.

The different stages of evaporative cooling are illustrated in Fig. 7. In the first stage (a) molecule formation is negligible. As the cooling process proceeds (b, c), an increasing part of the trapped sample consists of molecules. Here, it is important to note that the optical trap is twice as deep for the molecules. This is due to the weakly bound dimers having twice the polarizability. Therefore, evaporation in an atom-molecule mixture near thermal equilibrium essentially removes atoms and not the molecules. This predominant evaporation of unpaired atoms also has the interesting effect that the sample reaches a balanced 50/50 spin mixture, even if one starts the evaporation with some imbalance in the spin composition ([5]). In the final stage of the evaporation process, only molecules are left and the process can be essentially understood in terms of elastic molecule-molecule interactions. This leads to the formation of a molecular Bose-Einstein condensate (mBEC), as we will discuss in more detail in Sec. **4˙5**

We point out two more facts to fully understand the efficiency of the evaporative cooling process in our set-up. The magnetic field that we use for Feshbach tuning of the scattering properties [50] exhibits a curvature ([6]), which provides us with a magnetic trapping potential for the high-field seeking atoms along the laser beam axis (corresponding trapping frequency of $24.5\,\mathrm{Hz} \times \sqrt{B/\mathrm{kG}}$). When the optical trap is very week at the end of the evaporation process, the trap is a hybrid (optically for the transverse motion and magnetically for the axial motion). The cooling then results in an axial compression of the cloud which helps to maintain high enough number densities. The second interesting fact, which makes the all-optical route to degeneracy different for fermions and bosons [74, 68, 69, 75], is that evaporative cooling of fermions can be performed at very large scattering lengths. For bosons this is impossible because of very fast three-body decay [17, 68]. For a very large scattering length, a substantial part of the cooling process proceeds in the unitarity limit, where the scattering cross section is limited by the relative momentum of the particles. Decreasing temperature leads to an increase in the elastic scattering rate, which counteracts the effect of the decreasing number density when the sample is decompressed. Axial magnetic trapping and cooling in the unitarity limit help us to maintain the high elastic collision rate needed for a fast cooling process to degeneracy.

It is very interesting to compare evaporative cooling on the molecular side of the Feshbach resonance ($a < 0$) to the cooling on the other side of the resonance ($a > 0$). For similar values of $|a|$, one obtains a comparable cross section $\sigma = 4\pi a^2$ for elastic collisions between atoms in the two spin states. However, a striking difference shows up at low optical trap depth in the final stage of the evaporative cooling process. Fig. 8 shows how the number of trapped atoms (including the ones bound to molecules) decreases with the trap power. On the molecular side of the Feshbach resonance, a shallow trap can contain about ten times more atoms than on the other side of the resonance. Obviously, this cannot be understood in terms of the scattering cross section of atoms and highlights a dramatic dependence on the sign of the scattering length.

At the negative-a side of the resonance (open symbols in Fig. 8) a sharp decrease of the number of trapped particles is observed when the Fermi energy reaches the trap

---

([5]) A large initial imbalance, however, is detrimental as the cooling process already breaks down in the first stage where only atoms are present.

([6]) For technical reasons the coils were not realized in the Helmholtz configuration, where the curvature disappears. At the end this turned out to be a lucky choice for the creation of the mBEC.

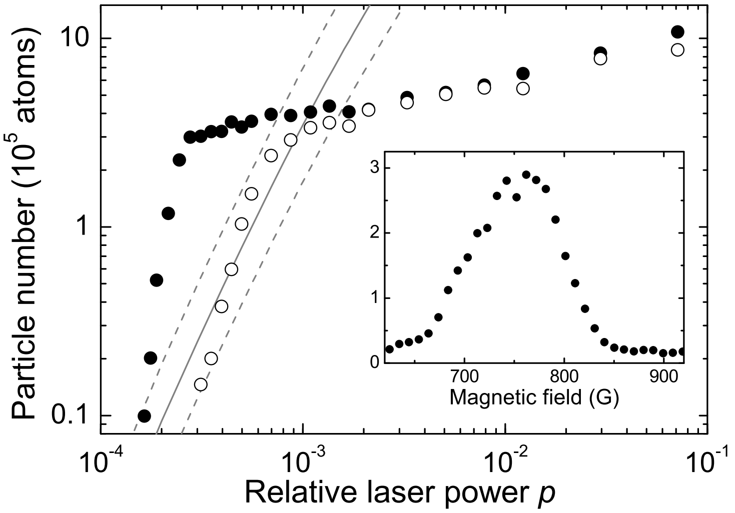

Fig. 8. – Evaporative cooling on both sides of the Feshbach resonance exhibits a strikingly different behavior [7]. The filled and open circles refer to magnetic fields of 764 G ($a = +4500a_0$) and 1176 G ($a = -3000\,a_0$). We plot the total number of trapped particles $2N_{\mathrm{mol}} + N_{\mathrm{at}}$ as a function of the laser power. The power p is given relative to the initial laser power of 10.5 W of an exponential evaporation ramp with a $1/e$ time constant of 230 ms; the corresponding initial trap depth for the atoms is $\sim 850\mu$K. The solid line shows the maximum number of trapped atoms according to the number of motional quantum states of the trap. The dashed lines indicate the corresponding uncertainty range due to the limited knowledge of the trap parameters. The inset shows the optimum production of molecules in the magnetic field range where a weakly bound molecular state exists. Here the total number of particles is measured for various magnetic fields at a fixed final ramp power $p = 2.8 \times 10^{-4}$, corresponding to a trap depth of $\sim$440 nK for the molecules.

depth. Lowering the trap power below this critical level leads to a spilling of atoms out of the trap. The trapping potential does simply not offer enough quantum states for the atoms. The observed spilling is consistent with the number of quantum states calculated for a non-interacting Fermi gas (solid line). A similar spilling effect is observed at the molecular side of the resonance ($a > 0$, filled symbols), but at much lower trap power. Before this spilling sets in, the trap contains nearly ten times more atoms as it would be possible for a non-interacting Fermi gas. This striking effect is explained by the formation and Bose-Einstein condensation of molecules. The spilling effect observed for the molecules with decreasing trap depth shows the chemical potential of the molecular condensate.

The strategy to evaporatively cool on the molecular side of the Feshbach resonance and to produce an mBEC as the starting point for further experiments is also followed at MIT, ENS, and Rice University. The Duke group performs forced evaporation very close to the resonance, which we believe to be a better strategy when the dynamical range for the trap power reduction is technically limited. Comparing the performance of evaporative cooling at different magnetic fields, we observed that the cooling process is somewhat more efficient and more robust on the molecular side of the resonance than very close to resonance.

4˙5. *The appearance of mBEC*. – At the time of our early mBEC experiments in fall 2003 [7] we had no imaging system to detect the spatial distribution of the gas at high magnetic fields, where we performed the evaporation experiments described in the preceding section. Nevertheless, by measuring the dependence of the total number of trapped particles on different parameters, we compiled various pieces of evidence for the formation of mBEC:

1. We observed that a very shallow trap can contain much more atoms than it offers quantum states for a weakly interacting atomic Fermi gas.
2. We observed very long lifetimes of up to 40 s for the trapped sample after a fast and highly efficient evaporation process. This shows that the sample has enough time to thermalize into an equilibrium state.
3. We measured the frequency of a collective oscillation mode (see also Sec. **6**), which clearly revealed hydrodynamic behavior.
4. By controlled spilling of the quantum gas out of the trap applying a variable magnetic gradient, we could demonstrate that the chemical potential of the trapped sample depends on the magnetic field in the way expected for a mBEC from the prediction of the dimer-dimer scattering lenghts, see Eq. 4.

These observations, together with our previous knowledge on molecule formation in the gas [26] and the general properties of the weakly bound dimers [56], led us to a consistent interpretation in terms of mBEC. At the same time mBEC was observed in a ^{40}K gas at JILA in Boulder [27]. It is an amazing coincidence that our manuscript was submitted for publication on exactly the same day (Nov. 3, 2003) as the Boulder work on mBEC in ^{40}K. Very shortly afterwards, the MIT group observed the formation of mBEC in ^{6}Li by detecting bimodal spatial distributions of the gas expanding after release from the trap [28]. A few weeks later, we observed the appearance of bimodial distributions in *in-situ* absorption images of the trapped cloud [32]. At about the same time also the ENS group reported on mBEC. Fig. 9 shows a gallery of different observations of bimodal distributions in formation of ^{6}Li mBECs at MIT [28], in Innsbruck [32], at ENS [29], and at Rice University [36].

5. – Crossover from mBEC to a fermionic superfluid

With the advent of ultracold Fermi gases with tunable interactions a unique way has opened up to explore a long-standing problem in many-body quantum physics, which has attracted considerable attention since the seminal work by Eagles [76], Leggett [77]

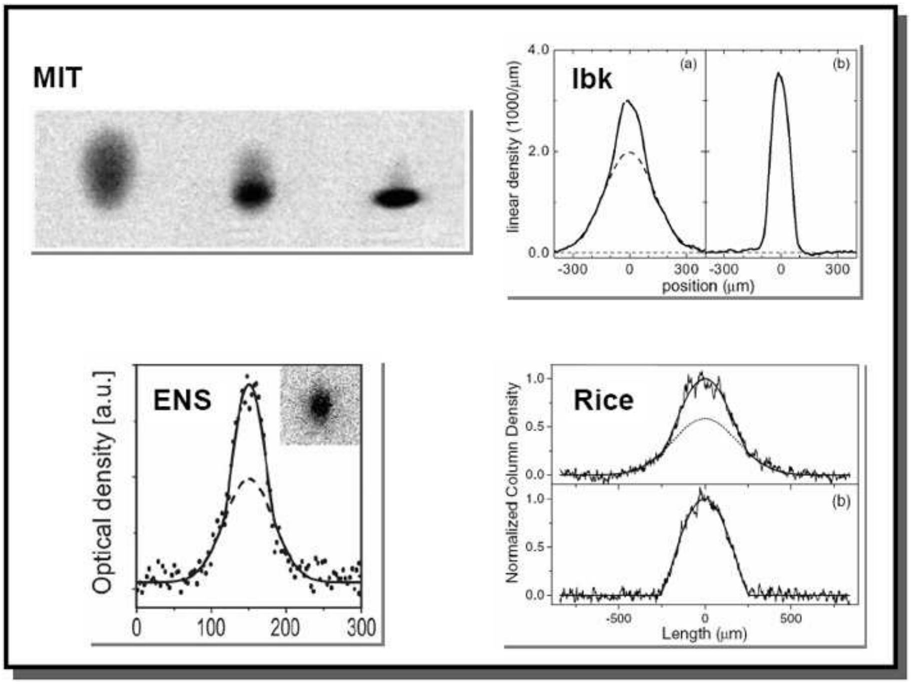

Fig. 9. – Gallery of ^{6}Li molecular BEC experiments. Bimodal spatial distributions were observed for expanding gases at MIT [28] and at ENS [29], and in *in-situ* profiles of the trapped cloud in Innsbruck [32] and at Rice University [36].

and Nozières and Schmitt-Rink [78]. Here we give a brief introduction (**5**˙1) into the physics of the BEC-BCS crossover (7) and we introduce some basic definitions and typical experimental parameters (**5**˙2). We then consider a universal Fermi gas with resonant interactions (**5**˙3) and the equation of state in the crossover (**5**˙4). Next we discuss the crossover at non-zero temperatures, including the isentropic conversion between different interaction regimes (**5**˙5). We finally review our first crossover experiments where we have observed how spatial profiles and the size of the strongly interacting, trapped cloud changed with variable interaction strength (**5**˙6).

5˙1. *BEC-BCS crossover physics: a brief introduction.* – The crossover of a superfluid system from the BEC regime into the Bardeen-Cooper-Schrieffer (BCS) regime can be

---

(7) In the condensed-matter literature, the crossover is commonly referred to as the "BCS-BEC crossover", because BCS theory served as the starting point. In our work on ultracold gases, we use "BEC-BCS crossover", because we start out with the molecular BEC. The physics is one and the same.

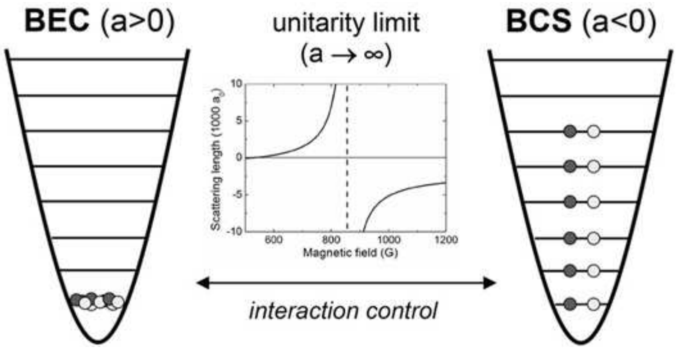

Fig. 10. – Illustration of the BEC-BCS crossover in a zero-temperature ^{6}Li Fermi gas with tunable interactions. For positive scattering length ($a > 0$, BEC side of the Feshbach resonance) the ground state of the system is a Bose-Einstein condensate of molecules. On resonance ($a \rightarrow \pm\infty$, unitarity limit) a strongly interacting Fermi gas with universal properties is realized. For negative scattering length ($a < 0$, BCS side of the resonance) the system approaches the BCS regime.

intuitively understood by first considering the two limits, which can be described in the framework of well-established theory (see illustration in Fig. 10). For moderate positive scattering lengths, the fermions form bosonic molecules, and the ground state at $T = 0$ is a BEC. For moderate negative scattering lengths, the ground state at $T = 0$ is the well-known BCS state [79, 80]. With variable interaction strength across a resonance, both regimes are smoothly connected through the strongly interacting regime. Here both BEC and BCS approaches break down and the description of the strongly interacting system is a difficult task. This situation poses great challenges for many-body quantum theories [81].

The nature of pairing is the key to understanding how the system changes through the crossover. On the BEC side, the pairs are molecules which can be understood in the framework of two-body physics. The molecular binding energy $E_{\rm b}$ is large compared with all other energies, and the molecules are small compared with the typical interparticle spacing. In this case, the interaction can be simply described in terms of molecule-molecule collisions, for which the scattering length is known (see **3**˙3). On the BCS side, two atoms with opposite momentum form Cooper pairs on the surface of the Fermi sphere. The pairing energy, i.e. the "pairing gap", is small compared with the Fermi energy $E_{\rm F}$ and the Cooper pairs are large objects with a size greatly exceeding the typical interparticle spacing. In the strongly interacting regime, the pairs are no longer pure molecules or Cooper pairs. Their binding energy is comparable to the Fermi energy and their size is about the interparticle spacing. One may consider them either as generalized molecules, stabilized by many-body effects, or alternatively as generalized Cooper pairs.

The ground state at $T = 0$ is a superfluid throughout the whole crossover. In the BEC limit, the fermionic degrees of freedom are irrelevant and superfluidity can be fully understood in terms of the bosonic nature of the system. In the opposite limit, superfluidity is described in the framework of BCS theory [79, 80]. In the strongly interacting regime, a novel type of superfluidity ("resonance superfluidity" [82, 83]) occurs where both bosonic and fermionic degrees of freedom are important .

5˙2. *Basic definitions, typical experimental parameters.* – Let us start with some basic definitions, which we will need to describe the physics in the rest of this contribution. The *Fermi energy* of a trapped, non-interacting two-component gas is given by

$$E_\mathrm{F} = \hbar\bar{\omega}\,(3N)^{1/3}\,, \tag{8}$$

here N is the total number of atoms in both spin states, and $\bar{\omega} = (\omega_\mathrm{x}\omega_\mathrm{y}\omega_\mathrm{z})^{1/3}$ is the geometrically averaged oscillation frequency in the harmonic trapping potential. This expression can be derived within the Thomas-Fermi approximation for a sufficiently large number of trapped atoms [84]. The chemical potential μ of the non-interacting gas is equal to E_F.

We use the Fermi energy of a non-interacting gas E_F to define an *energy scale* for the whole BEC-BCS crossover, i.e. for any regime of interactions. The corresponding Fermi temperature is

$$T_\mathrm{F} = E_\mathrm{F}/k_\mathrm{B}\,. \tag{9}$$

We now introduce a Fermi wave number k_F, following the relation

$$\frac{\hbar^2 k_\mathrm{F}^2}{2m} = E_\mathrm{F}\,. \tag{10}$$

The inverse Fermi wave number k_F^{-1} defines a typical *length scale* for the crossover problem. For the non-interacting case, k_F is related to the peak number density n_0 in the center of the trap [84] by

$$n_0 = \frac{k_\mathrm{F}^3}{3\pi^2}\,. \tag{11}$$

To characterize the interaction regime, we introduce the dimensionless interaction parameter $1/k_\mathrm{F}a$, which is commonly used to discuss crossover physics. We can now easily distinguish between three different regimes. The BEC regime is realized for $1/k_\mathrm{F}a \gg 1$, whereas the BCS regime is obtained for $1/k_\mathrm{F}a \ll -1$. The strongly interacting regime lies between these two limits where $1/k_\mathrm{F}|a|$ being small or not greatly exceeding unity.

Let us consider typical experimental parameters for our ^{6}Li spin mixture: an atom number N of a few 10^5, and a mean trap frequency $\bar{\omega}/2\pi$ near 200 Hz. This corresponds to a typical Fermi temperature $T_\mathrm{F} \approx 1\,\mu$K and to $k_\mathrm{F}^{-1} \approx 200\,\mathrm{nm} \approx 4000\,a_0$. A comparison of k_F^{-1} with the scattering lengths close to the 834 G Feshbach resonance (see Fig. 2) shows that there is a broad crossover region where the ^{6}Li system is strongly interacting. The peak number then considerably exceeds the typical value $n_0 \approx 4 \times 10^{12}\,\mathrm{cm}^{-3}$ calculated for the non-interacting case.

5˙3. *Universal Fermi gas in the unitarity limit.* – The resonance where $a(B)$ diverges and $1/k_\mathrm{F}a = 0$, is at the heart of BEC-BCS crossover physics ([8]). Here the s-wave interaction between colliding fermions is as strong as quantum mechanics allows within the fundamental limit of unitarity. In this situation, E_F and $1/k_\mathrm{F}$ represent the only energy and length scales in the problem and the system acquires universal properties [85, 86, 87]. The broad Feshbach resonance in the ultracold ^{6}Li gas offers excellent possibilities to study the properties of the universal Fermi gas [88] and the situation has attracted a great deal of experimental interest, as described in various parts of these proceedings.

At $T = 0$, universality implies a simple scaling behavior with respect to the situation of a non-interacting Fermi gas. Following the arguments in Refs. [85, 86, 21] the atomic mass m can be simply replaced by an effective mass

$$m_\mathrm{eff} = \frac{m}{1+\beta}\,, \tag{12}$$

where $\beta \simeq -0.57$ [89, 90] is a dimensionless, universal many-body parameter. For a harmonic trapping potential, Eq. 12 results in an effective trap frequency $\bar{\omega}_\mathrm{eff} = \sqrt{1+\beta}\,\bar{\omega}$, and the chemical potential for zero-temperature gas in the unitarity limit is then given by

$$\mu = \sqrt{1+\beta}\,E_\mathrm{F}\,. \tag{13}$$

The density profile of the universal Fermi gas with resonant interactions is just a simple rescaled version of the density profile of the non-interacting gas, smaller by a factor of $(1+\beta)^{1/4} \simeq 0.81$.

The universal many-body parameter was recently calculated based on quantum Monte-Carlo methods, yielding $\beta = -0.56(1)$ [89] and $-0.58(1)$ [90]. A diagrammatic theoretical approach [91] gave a value -0.545 very close to these numerical results. Several experiments in ^{6}Li [32, 29, 37, 39] and in ^{40}K [92] have provided measurements of β in good agreement with the theoretical predictions. We will discuss our experimental results on β in some more detail in **5**˙6.

At $T \neq 0$, the Fermi gas with unitarity-limited interactions obeys a universal thermodynamics with T/T_F being the relevant dimensionless temperature parameter [87]. Thermodynamic properties of the system have been experimentally studied in Ref. [37].

([8]) In nuclear physics this situation is known as the “Bertsch problem”. G. F. Bertsch raised the question on the ground state properties of neutron matter under conditions where the scattering length between the two neutron spin states is large compared to the interparticle spacing.

5˙4. *Equation of state.* – The equation of state is of central interest to characterize the interaction properties of the Fermi gas in the BEC-BCS crossover. For a system at $T = 0$, the equation of state is described by the chemical potential μ as a function of the number density n. For $\mu(n)$ at $T = 0$, we now consider three special cases. For a non-interacting Fermi gas, $\mu = E_\mathrm{F}$, and one thus obtains

$$\mu = (3\pi^2)^{2/3}\frac{\hbar^2}{2m}\,n^{2/3}\,. \tag{14}$$

For a Fermi gas with resonant interactions, universality implies that one obtains the same expression with a prefactor $1+\beta$ (Eq. 12). In the mBEC regime, the chemical potential for the dimers is $\mu_\mathrm{d} = 4\pi\hbar^2 a_\mathrm{dd} m_\mathrm{d}^{-1}\,n_\mathrm{d}$. With the simple relations between mass ($m_\mathrm{d} = 2m$), number density ($n_\mathrm{d} = n/2$), and scattering length ($a_\mathrm{dd} = 0.6a$, see Eq. 4) for dimers and atoms, and after substraction of the molecular binding energy E_b $= \hbar^2/(ma^2)$, we obtain

$$\mu = \frac{1}{2}\left(\mu_\mathrm{d} - E_\mathrm{b}\right) = \frac{\hbar^2}{2m}\left(0.6\pi\,a\,n - a^{-2}\right)\,. \tag{15}$$

For the general BEC-BCS crossover problem one can introduce a "polytropic" equation of state [93] in the form

$$\mu \propto n^\gamma\,. \tag{16}$$

Here the "polytropic index" γ depends on the interaction parameter $1/k_\mathrm{F}a$. By comparing this equation of state with the above expressions one immediately sees that $\gamma = 1$ for the mBEC case ($1/k_\mathrm{F}a \gg 1$), $\gamma = 2/3$ both for the unitarity limit ($1/k_\mathrm{F}a = 0$) and for the non-interacting case ($1/k_\mathrm{F}a \ll -1$). These three values are fixed boundary conditions for any crossover theory describing γ as a function of $1/k_\mathrm{F}a$.

In the experiments, the Fermi gases are usually confined in nearly harmonic trapping potentials, which leads to an inhomogeneous density distribution. If the trap is not too small one can introduce the *local-density approximation* and consider a local chemical potential $\mu(\mathbf{r}) = \mu - U(\mathbf{r})$, which includes the trapping potential $U(\mathbf{r})$ at the position $\mathbf{r}$. This assumption holds if the energy quantization of the trap is irrelevant with respect to the chemical potential and the pair-size is small compared to the finite size of the trapped sample. This approximation is well fulfilled for all crossover experiments performed in Innsbruck.

5˙5. *Phase-diagram, relevant temperatures and energies.* – At finite temperatures the BEC-BCS crossover problem becomes very challenging and it is of fundamental interest to understand the phase diagram of the gas. Two temperatures play an important role, the temperature T_c for the superfluid phase transition and a pairing temperature T^*, characterizing the onset of pairing. Let us first discuss these two temperatures in the three limits of the crossover (BEC, unitarity, and BCS), see first two rows in Table I.

TABLE I. – *Overview of important temperatures and energies in the three crossover limits. The expressions are valid for a harmonically trapped Fermi gas.*

		mBEC $(1/k_{\mathrm{F}}a \gg 1)$	unitarity $(1/k_{\mathrm{F}}a = 0)$	BCS $(1/k_{\mathrm{F}}a \ll -1)$
crit. temp.	T_{c}	$0.518\,T_{\mathrm{F}}$	$\sim 0.3\,T_{\mathrm{F}}$	$0.277\,T_{\mathrm{F}} \exp\left(\frac{\pi}{2k_{\mathrm{F}}a}\right)$
pair. temp.	T^*	$12\left(\frac{T}{T_{\mathrm{F}}}\right)^3 = \exp\left(\frac{T_F}{T}\,\frac{2}{(k_{\mathrm{F}}a)^2}\right)$	$\sim 0.4\,T_{\mathrm{F}}$	T_{c}
gap energy	2Δ	$2\,(k_{\mathrm{F}}a)^{-2}E_{\mathrm{F}}$	$1.8E_{\mathrm{F}}$	$3.528\,k_{\mathrm{B}}T_{\mathrm{c}}$
chem. pot.	μ	$\left(0.294(k_{\mathrm{F}}a)^{2/5} - (k_{\mathrm{F}}a)^{-2}\right)E_{\mathrm{F}}$	$0.66E_{\mathrm{F}}$	E_{F}

The critical temperature T_{c} in the mBEC limit follows directly from the usual expression for the BEC transition temperature in a harmonic trap $k_{\mathrm{B}}T_{\mathrm{c}} \simeq 0.94\hbar\bar{\omega}N_{\mathrm{m}}^{1/3}$ [94], $N_{\mathrm{m}} = N/2$, and $k_{\mathrm{B}}T_{\mathrm{F}} = \hbar\bar{\omega}(3N)^{1/3}$. The given value for the critical temperature in the unitarity limit was derived in various crossover theories [95, 37]. For the BCS regime, the critical temperature is a well-known result from Ref. [96]; see also Refs. [97, 98].

For the pairing temperature T^*, typical numbers are given in the second row of Table I. In the framework of BCS theory, there is no difference between T^* and T_{c}, which means that as soon as Cooper pairs are formed the system is also superfluid. On the BEC side, however, molecules are formed at much higher temperatures as the phase transition to molecular BEC occurs (see discussion in **4**˙3). Setting $\phi_{\mathrm{mol}} = \phi_{\mathrm{at}}$ in Eq. 7, one can derive the implicit equation for T^*/T_{F} given in the Table. In the unitarity limit, T^* is not much higher than T_{c}; Ref. [95] suggests $T^*/T_{\mathrm{c}} \approx 1.3$.

The phase diagram in Fig. 11 illustrates the behavior of T_{c} and T^*, as discussed before for the three limits. We point out that, in strongly interacting Fermi gases, there is a certain region where pairing occurs without superfluidity. In the language of high-T$_{\mathrm{c}}$ superconductivity [99, 81], "preformed pairs" are present in the "pseudo-gap regime".

For overview purposes, Table I also gives the pairing energy 2Δ and the chemical potential μ. In the mBEC regime, the pairing energy just corresponds to the molecular binding energy $E_{\mathrm{b}} = 2(k_{\mathrm{F}}a)^{-2}E_{\mathrm{F}}$. The chemical potential $\mu = \frac{1}{2}(\mu_{\mathrm{d}} - E_{\mathrm{b}})$ (see Eq. 15) can be derived from $\mu_{\mathrm{d}}/\hbar\bar{\omega} = \frac{1}{2}(15N_{\mathrm{d}}a_{\mathrm{d}}/a_{\mathrm{ho}})^{2/5}$ with $a_{\mathrm{ho}} = (\hbar/m_{\mathrm{d}}\bar{\omega})^{1/2}$, valid for an mBEC in the Thomas-Fermi limit [94]. In the BCS limit, there is the fixed relation of the "gap" Δ to the critical temperature T_{c} given in Table I. For the unitarity limit, the value given for the pairing energy stems from quantum Monte-Carlo calculations [89]. The behavior of Δ in the crossover is extensively discussed in **7**˙3. The table also presents the chemical potential μ according to Eqs. 14 and 15, rewritten in terms of the parameters $1/k_{\mathrm{F}}a$ and E_{F}.

5˙6. *First Innsbruck crossover experiments: conservation of entropy, spatial profiles, and potential energy of the trapped gas.* – The possibility to continuously vary the interaction parameter $1/k_{\mathrm{F}}a$ through Feshbach tuning offers the fascinating possibility to convert the Fermi gas between different regimes and thus to explore the BEC-BCS

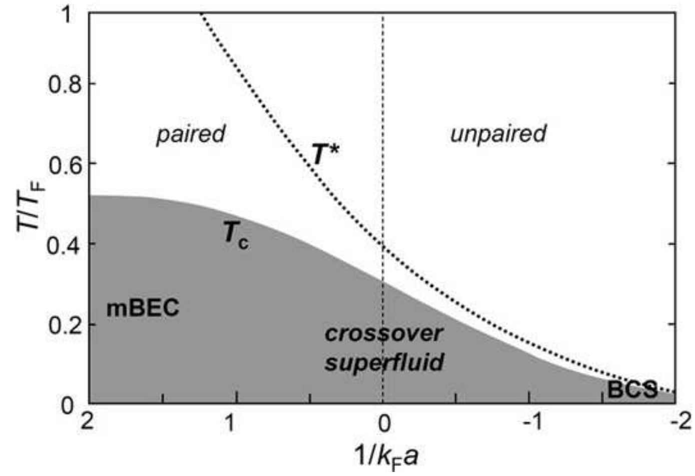

Fig. 11. – Schematic phase diagram for the BEC-BCS crossover in a harmonic trapping potential [95]. The critical temperature T_c marks the phase transition from the normal to the superfluid phase. Pair formation sets in gradually at a typical temperature $T^* > T_\mathrm{c}$.

crossover. We performed our first experiments on crossover physics [32] in December 2003 shortly after the first creation of the mBEC [7]. Here we summarize the main results of these early experiments, which are of general importance for BEC-BCS crossover experiments with ^{6}Li.

We performed slow conversion-reconversion cycles, in which the strongly interacting gas was adiabatically converted from the BEC side of the crossover to the BCS side and vice versa. We found that this conversion took place in a lossless way and that the spatial profiles of the trapped cloud did not show any significant heating. We could thus demonstrate that, under appropriate experimental conditions, the conversion process can proceed in an essentially *adiabatic and reversible* way, which means that the *entropy* of the gas is conserved.

The conservation of entropy has important consequences for the experiments: Because of the different relations between entropy and temperature in various interaction regimes, an isentropic conversion in general changes the temperature. As a substantial benefit, a drastic temperature reduction occurs when the degenerate gas is converted from mBEC into the BCS regime. This is very favorable for the achievement of a superfluid state on the BCS side of the resonance [98] or in the unitarity-limited resonance regime [100]. In our experiments, we typically start out with a condensate fraction of more than 90% in the weakly interacting mBEC regime. Based on the isentropic conversion process and the thermodynamics discussed in Ref. [100] we estimate that we obtain typical temperatures

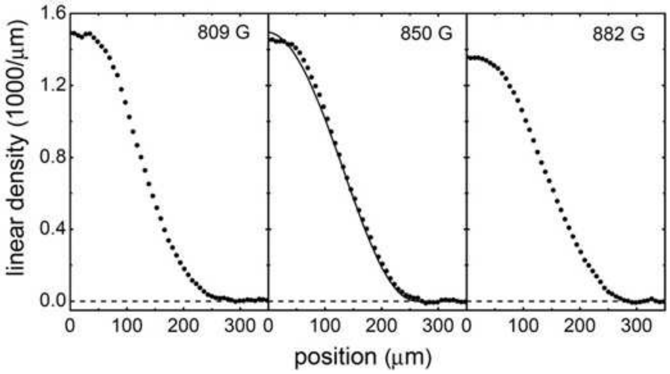

Fig. 12. – Axial density profiles of a trapped ^{6}Li Fermi gas in the crossover region [32]. The middle profile, taken very close to resonance (850 G), is compared to the Thomas-Fermi profile of a universal Fermi gas (solid line). The small deviation on the top is due to a residual interference pattern in the images.

between $0.05\,T_\mathrm{F}$ and $0.1\,T_\mathrm{F}$ for the Fermi gas in the unitarity limit (^{9}).

Using slow magnetic field ramps we isentropically converted the trapped gas into different interaction regimes covering the whole resonance region and beyond. By *in-situ* imaging we recorded the axial density profiles of the trapped cloud. The results (see profiles in Fig. 12) demonstrated the smooth behavior in the crossover. The cloud just became larger without showing any particular features, and we found simple Thomas-Fermi profiles to fit our observations very well. The one-dimensional spatial profiles did not show any signatures of a superfluid phase transition (^{10}), in agreement with theoretical expectations [95, 101].

To quantitatively characterize the behavior, we measured the root-mean-square axial size z_rms of the cloud as a function of the magnetic field B. The normalized quantity $\zeta = z_\mathrm{rms}/z_0$ gives the relative size as compared to a non-interacting Fermi gas, where $z_0 = (E_\mathrm{F}/4m\omega_z^2)^{1/2}$. The *potential energy* of the harmonically trapped gas relative to a non-interacting Fermi gas is then simply given by ζ^2. Within the local density approximation, this is also valid for the three-dimensional situation. Our experimental results can thus be interpreted as the first measurements of the potential energy of a trapped Fermi gas near $T = 0$ in the BEC-BCS crossover (^{11}).

(^{9}) We note that the large stability of ^{6}Li in the mBEC regime offers an advantage over ^{40}K in that one can evaporatively cool in the mBEC regime and exploit the temperature-reduction effect in conversion onto the BCS side of the resonance.

(^{10}) This is different in an imbalanced spin-mixture, where the superfluid phase transition was observed by changes in the spatial profiles [41].

(^{11}) We note that a later thorough analysis of the conditions of the experiments in Ref. [32] confirmed the atom number $N = 4 \times 10^5$ to within an uncertainty of ±30%. However, we found that the horizontal trap frequency was only 80% of the value that we used based on

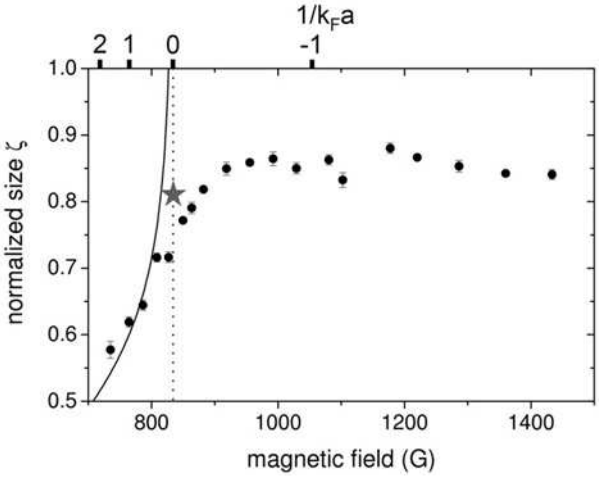

Fig. 13. – Results of the first Innsbruck BEC-BCS crossover experiments [32] on the axial size normalized to the theoretical size of a non-interacting Fermi gas ($\zeta = z_{\rm rms}/z_0$). The solid line is a theoretical prediction for the size of a mBEC in the Thomas-Fermi limit, and the star indicates the theoretical value for the unitarity limit.

The measured values for the relative size ζ are plotted in Fig. 13 and compared to the predictions for a weakly interacting molecular BEC with $a_{\rm dd} = 0.6a$ in the in the Thomas-Fermi limit (solid line) and a universal Fermi gas in the unitarity limit (star). The experimental data on the mBEC side are consistent with the theoretical prediction. On resonance, the measured size was found somewhat below the prediction $(1+\beta)^{1/4} \simeq 0.81$ (**5**˙3); see star in Fig. 13. This slight discrepancy, however, may be explained by possible calibration errors in the measured number of atoms and in the magnification of the imaging system in combination with the anharmonicity of the radial trapping potential. Beyond resonance the results stayed well below the non-interacting value $\zeta = 1$, showing that we did not reach weakly interacting conditions, This is a general consequence of the large background scattering length of ^{6}Li, which (in contrast to ^{40}K) makes it very difficult to realize a weakly interacting Fermi gas on the BCS side of the Feshbach resonance.

In general, the dependence of the size and thus the potential energy of the trapped gas in the BEC-BCS crossover that we observed in our first experiments [32] was found to fit well to corresponding theoretical predictions [91]. Later experiments by other groups provided more accurate measurements on the size of the gas for the particulary

---

the assumption of a cylindrically symmetric trap (see **6**˙4). Moreover, the exact position of the Feshbach resonance was located at 834 G (see **3**˙2) instead of 850 G as assumed in the first analysis of the experiment. The up-to-date values are used for Fig. 13, causing slight deviations from the original presentation of our data.

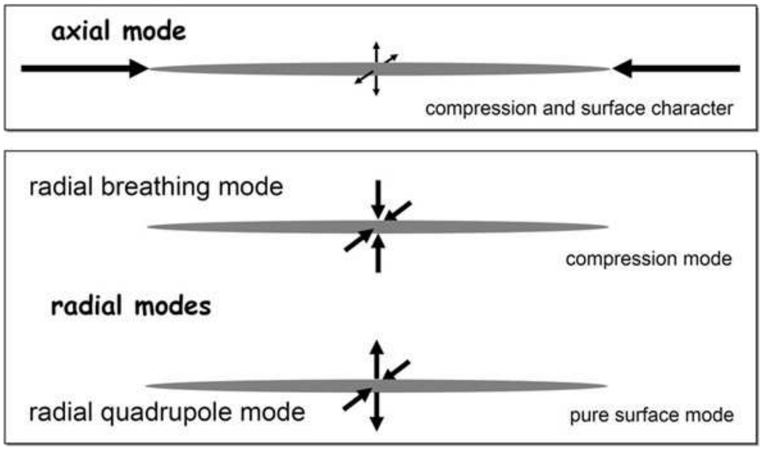

Fig. 14. – Illustration of elementary collective modes of a cigar-shaped quantum gas, confined in an elongated trap. The axial mode corresponds to a slow oscillation with both compression and surface character. The two low-lying radial modes correspond to fast oscillations with strong compression character ("radial breathing mode") and with pure surface character ("radial quadrupole mode").

interesting unitarity limit [37, 39, 92].

6. – Collective excitations in the BEC-BCS crossover

Elementary excitation modes provide fundamental insight into the properties of quantum-degenerate gases. In particular, they provide unique experimental access to study the hydrodynamic behavior that is associated with superfluidity. Collective modes have been studied very early in atomic BEC research, both in experiments [102, 103] and in theory [104]. Measurements on collective oscillations have proven powerful tools for the investigation of various phenomena in atomic BECs [105, 106, 107, 108, 109]. Building on this rich experience, collective modes attracted immediate attention to study strongly interacting Fermi gases [110, 33, 34] as soon as these systems became experimentally available. Here, we give a basic introduction into collective modes in the BEC-BCS crossover (**6**˙1), and we present an overview of the major experimental results obtained in our laboratory in Innsbruck and at Duke University (**6**˙2), before we discuss our results in some more detail (**6**˙3–**6**˙6).

6˙1. *Basics of collective modes.* – We will focus our discussion on the geometry of elongated traps with cylindrical symmetry, because this is the relevant geometry for strongly interacting Fermi gases in single-beam optical traps. Besides the simple sloshing modes that correspond to center-of-mass oscillations in the trap, the cigar-shaped quantum gas exhibits three elementary, low-lying collective modes, which are illustrated in Fig. 14.

The *axial mode* corresponds to an oscillation of the length of the "cigar" with a frequency of the order of the axial trap frequency ω_{z}. This oscillation is accompanied by a 180° phase-shifted oscillation of the cigar's radius, which reflects a quadrupolar character of the mode. Thus, the mode has the mixed character of a compression and a surface mode. The frequencies of the two low-lying *radial modes* are of the order of the radial trap frequency ω_{r}. The "radial breathing mode" is a compression mode, for which the radius of the sample oscillates. The "radial quadrupole mode" is a pure surface mode where a transverse deformation oscillates without any change of the volume.

To understand collective modes in a Fermi gas, it is crucial to distinguish between two fundamentally different regimes. Which regime is realized in an experiment depends on the interaction strength $1/k_{\mathrm{F}}a$ and the temperature T of the gas.

- *The collisionsless, non-superfluid regime* – In a weakly interacting degenerate Fermi gas, elastic collisions are Pauli blocked [111, 112, 113]. This is due to the fact that the final states for elastic scattering processes are already occupied. This Pauli blocking effect has dramatic consequences for the dynamics of a two-component Fermi gas when it is cooled down to degeneracy. In the non-degenerate case, the influence of collisions between the two different spin states can be very strong, as it is highlighted by our efficient evaporative cooling process (see **4**˙3). In the degenerate case, however, collisions are strongly suppressed. A substantial increase in relaxation times [114] shows up as an important consequence.

- *The hydrodynamic regime* – When a superfluid is formed at sufficiently low temperatures, hydrodynamic behavior occurs as an intrinsic property of the system, and the gas follows the equations of *superfluid hydrodynamics* (see lecture of S. Stringari in these proceedings). However, in a strongly interacting Fermi gas bosonic pairs can be formed and their elastic interactions are no longer Pauli blocked; this may lead to *classical hydrodynamics* in a degenerate gas. In this case, the sample follows basically the same hydrodynamic equations as in the superfluid case. Therefore, it is not possible to draw an immediate conclusion on superfluidity just from the observation of hydrodynamic behavior.

The existence of these two different regimes has important consequences for collective oscillations. In the (non-superfluid) collisionless case, the fermionic atoms perform independent oscillations in the trapping potential and the effect of elastic collisions and collisional relaxation is small [115, 114]. The ensemble then shows decoupled oscillations along the different degrees of freedoms with frequencies that are twice the respective trap frequencies (12).

In the hydrodynamic regime, a solution of the equations of motion (see lecture of S. Stringari) yields the following expressions for the collective mode frequencies in the

---

(12) We neglect small interaction shifts, which are discussed in [115].

TABLE II. – *Overview of collective mode frequencies in different regimes.*

		hydrodynamic		*collisionless,*
		mBEC $(1/k_\mathrm{F}a \gg 1)$	unitarity $(1/k_\mathrm{F}a = 0)$	*non-superfluid*
axial mode	$\omega_\mathrm{ax}/\omega_\mathrm{z}$	$\sqrt{5/2} = 1.581..$	$\sqrt{12/5} = 1.549..$	2
radial compression mode	$\omega_\mathrm{c}/\omega_\mathrm{r}$	2	$\sqrt{10/3} = 1.826..$	2
radial quadrupole mode	$\omega_\mathrm{q}/\omega_\mathrm{r}$	$\sqrt{2} = 1.414..$	$\sqrt{2} = 1.414..$	2

elongated trap limit, $\omega_\mathrm{z}/\omega_\mathrm{r} \rightarrow 0$ (13):

$$\omega_\mathrm{ax} = \sqrt{(3\bar{\gamma}+2)/(\bar{\gamma}+1)}\;\omega_\mathrm{z}\,, \tag{17}$$

$$\omega_\mathrm{c} = \sqrt{2\bar{\gamma}+2}\;\omega_\mathrm{r}\,, \tag{18}$$

$$\omega_\mathrm{q} = \sqrt{2}\;\omega_\mathrm{r}\,. \tag{19}$$

Here $\bar{\gamma}$ is an effective polytropic index for the equation of state (Eq. 16), which takes into account the variation of the density across the inhomogeneous sample in the harmonic trap [116, 117]. For the mBEC case $\bar{\gamma} = 1$, and for the unitarity limit $\bar{\gamma} = 2/3$. The theory of collective modes in the BEC-BCS crossover has attracted considerable interest and is extensively discussed in Refs. [110, 93, 116, 118, 119, 120, 121, 117, 122, 123].

Table II presents an overview of the frequencies of the three low-lying modes in different regimes. When the interaction is varied from mBEC to the unitarity limit, the axial mode changes its frequency by just ∼2%. However, for the radial breathing mode the relative change is five times larger (∼10%). This difference reflects the much stronger compression character of the radial breathing mode, which is why this mode is a prime tool to experimentally investigate the equation of state (see **6**˙5). The fact that the radial quadrupole mode is a pure surface mode makes it insensitive to the equation of state. This mode can thus serve as a powerful tool for investigating the large differences between hydrodynamic and collisionless behavior [124].

6˙2. *Overview of recent experiments.* – Here we give a brief overview of the major results of collective mode experiments performed at Duke University and in Innsbruck. Already in our early work on mBEC [7] we measured the axial mode frequency to show that the trapped sample behaved hydrodynamically. The first experimental results on collective modes in the BEC-BCS crossover were reported by our team and the Duke group at the *Workshop on Ultracold Fermi Gases* in Levico (4-6 March 2004). These results were published in Refs. [33, 34].

The Duke group investigated the radial breathing mode for resonant interactions and

---

(13) For all experiments reported here, the traps fulfilled $\omega_\mathrm{z}/\omega_\mathrm{r} < 0.1$, which makes the elongated trap limit a valid approximation.

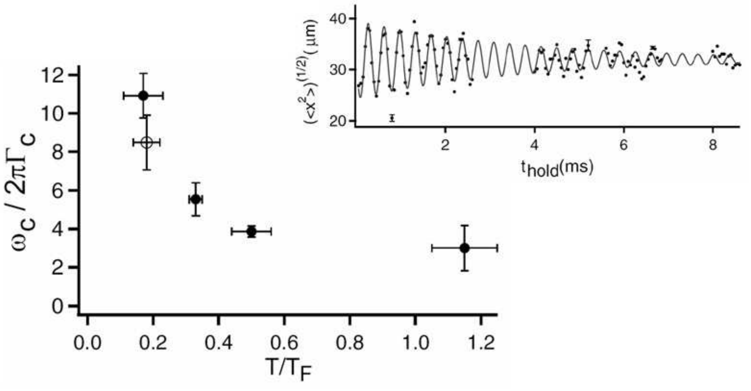

Fig. 15. – Evidence for superfluidity in a strongly interacting Fermi gas obtained at Duke University from measurements of the damping of the radial breathing mode [33]. The damping time $1/\Gamma_c$ (in units of the oscillation period $2\pi/\omega_c$) is plotted versus temperature T. The inset shows a breathing oscillation ($\omega_c/2\pi = 2830\,\mathrm{Hz}$) at the lowest temperatures reached in the experiment. This figure was adapted from Ref. [33].

measured a frequency that was consistent with the theoretical prediction (see **6**˙1) for a hydrodynamic Fermi gas with unitarity-limited interactions. They also investigated the temperature-dependent damping behavior and observed strongly increasing damping times when the sample was cooled well below the Fermi temperature T_F; the main result is shown in Fig. 15. By comparing the results with available theories on Fermi gases in the collisionless, non-superfluid regime and with theories on collisional hydrodynamics they found the observed behavior to be inconsistent with these two regimes [33]. Superfluidity provided a plausible explanation for these observations, and the Duke group thus interpreted the results as *evidence for superfluidity.* Later experiments [35, 37, 38] indeed provided a consistent picture of superfluidity for the conditions under which these collective mode experiments were performed.

In our early experiments [34], we measured the frequencies of the axial mode and the radial compression mode in the BEC-BCS crossover. Here we observed the frequency variations that result from the changing equation of state. On the BCS side of the Feshbach resonance, we observed a transition from hydrodynamic to non-superfluid, collisonless behavior. The transition occurred rather smoothly in the axial mode (see **6**˙3) but abruptly in the radial breathing mode (see **6**˙4). We also observed ultralow damping in the axial mode, which nicely fits into the picture of superfluidity. The abrupt breakdown of hydrodynamics in the radial breathing mode was also observed at Duke University [125].

Further experiments on collective modes at Duke University [126] provided more information on the temperature dependence of damping for unitarity-limited interactions. This experiment also hinted on different damping regimes. At Innsbruck University, we carried out a series of precision measurements on the frequencies of collective modes in

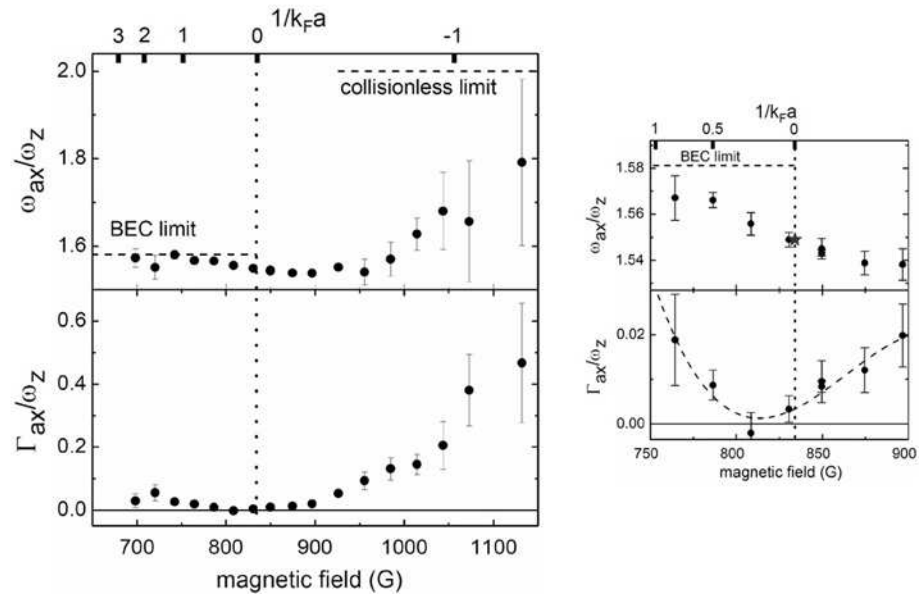

Fig. 16. – Axial mode in the BEC-BCS crossover. The figure shows our measurements [34] of the frequency $\omega_{\rm ax}$ and the damping rate $\Gamma_{\rm ax}$ in units of the axial trap frequency $\omega_{\rm z}$ ($\omega_{\rm z}/2\pi = 22.6\,$Hz at $B = 834\,$G, $\omega_{\rm r}/2\pi \approx 700\,$Hz). The horizontal, dashed lines indicate the theoretically expected frequencies in the BEC limit and in the collisionless limit (cf. Table II). The figure on the right-hand side shows a blow-up of the resonance region; here the star refers to the frequency expected for the unitarity limit.

the crossover [71]. This provided a test of the equation of state and resolved seeming discrepancies between state-of-the-art theoretical predictions [117] and the early experiments [34, 125].

6˙3. *Axial mode.* – Our measurements of frequency and damping of the axial mode [34] are shown in Fig. 16. To tune the two-body interaction we varied the magnetic field in a range between 700 and 1150 G, corresponding to a variation of the interaction parameter $1/k_{\rm F}a$ between 2.5 and -1.2. For magnetic fields up to ∼900 G ($1/k_{\rm F}a \approx -0.45$), the oscillation shows the hydrodynamic frequencies and very low damping. For higher fields, damping strongly increases and the frequency gets closer to the collisionless value, but never reaches it completely. These observations are consistent with a gradual transition from hydrodynamic to collisionless behavior [114]. Even far on the BCS side of the resonance, the true collisionless regime is not reached, as the Pauli blocking effect is not strong enough to suppress elastic collisions on a time scale below the very long axial oscillation period of about 50 ms.

At the right-hand side of Fig. 16, we show a blow-up of the resonance region. One clearly sees that the axial mode frequency changes from the BEC value $\omega_{\rm ax}/\omega_{\rm z} = \sqrt{5/2} = 1.581$ to the value of a universal Fermi gas in the unitarity limit of $\sqrt{12/5} = 1.549$. We were able to detect this small 2% effect because of the very low damping of the mode, allowing long observation times. Moreover, the magnetic axial confinement was perfectly harmonic, and the corresponding trap frequency ω_z could be measured with a relative uncertainty of below 10^{-3} [127].

It is also very interesting to consider the damping of the axial mode. The minimum damping rate was observed at $\sim$815 G, which is slightly below the exact resonance (834 G). Here we measured the very low value of $\Gamma_\mathrm{z}/\omega_\mathrm{z} \approx 0.0015$, which corresponds to a $1/e$ damping time as large as $\sim$5 s. According to our present knowledge of the system, this ultralow damping is a result of superfluidity of the strongly interacting Fermi gas. The damping observed for lower magnetic fields can be understood as a consequence of heating due to inelastic processes in the gas ([14]). In general, damping rates are very sensitive to the residual temperature of the sample.

6·4. *Radial breathing mode: breakdown of hydrodynamics.* – Our early measurements [34] of frequency and damping of the radial breathing mode are shown in Fig. 17. The most striking feature is a sharp transition from the hydrodynamic to the collisionless regime. This occurs at a magnetic field of $\sim$900 G ($1/k_\mathrm{F}a \approx -0.45$). Apparently, the hydrodynamic regime extends from the mBEC region across the unitarity limit onto the BCS side of the resonance. This behavior is consistent with the direct observation of superfluidity in the crossover region through vortices [38]. The breakdown of superfluid hydrodynamics is accompanied by very fast damping, which indicates a fast dissipation mechanism in the sample. We will come back to this in our discussion of the pairing gap (last paragraph in **7**·3). The breakdown of hydrodynamics on the BCS side of the resonance was also observed by the Duke group [125].

To quantitatively understand the frequencies in the hydrodynamic regime as measured in our early collective mode experiments [34], one has to take into account an unintended ellipticity of the transverse trapping potential [128]. We found out later after technical upgrades to our apparatus that the ratio of horizontal and vertical trap frequencies was $\omega_\mathrm{x}/\omega_\mathrm{y} \approx 0.8$. Due to the fact that the gas was not completely cylindrically symmetric, the collective mode frequencies deviate from the simple expressions presented in **6**·1. For small ellipticities, Eq. 18 still provides a reasonable approximation when an effective transverse oscillation frequency of $\sqrt{\omega_\mathrm{x}\omega_\mathrm{y}}$ is used for ω_r [33]. For an accurate interpretation of the measurements, however, a more careful consideration of ellipticity effects is necessary [129, 71, 128].

In Fig. 17, we indicate the expected normalized compression mode frequencies $\omega_\mathrm{c}/\omega_\mathrm{y}$ for the limits of mBEC (dahed line below resonance), unitarity (star), and for a non-interacting collisionless gas (dashed line above resonance). For normalization we have used the vertical trap frequency ω_y, which was directly measured in the experiments. Moreover, we assumed $\omega_\mathrm{x}/\omega_\mathrm{y} = 0.8$ to calculate the eigenfrequencies of the collective

---

[14] Precise frequency measurements of the slow axial mode require long observation times. On the BEC side of the resonance, heating due to inelastic decay then becomes a hardly avoidable problem.

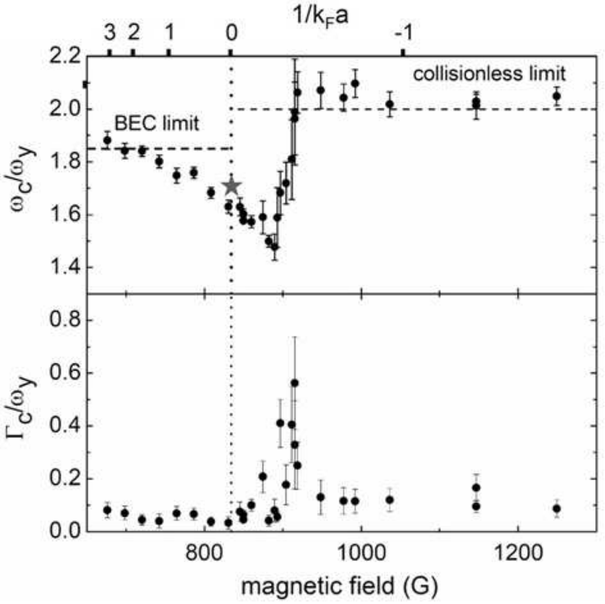

Fig. 17. – Measurements of the frequency ω_c and the damping rate Γ_c of the radial compression mode in the BEC-BCS crossover [34]. Here the oscillation frequencies were determined relative to the vertical trap frequency $\omega_y \approx 750\,\text{Hz}$. As we found in later experiments, the trap was somewhat elliptic with a horizontal trap frequency $\omega_x \approx 600\,\text{Hz}$. This is about 20% below the vertical one and has a substantial effect on the hydrodynamic frequencies [128]. On the BEC side of the Feshbach resonance, the dashed line indicates the frequency theoretically expected in the BEC limit ($\omega_c/\omega_y = 1.85$ for $\omega_x/\omega_y = 0.8$). The star marks the frequency in the unitarity limit ($\omega_c/\omega_y = 1.805$ for $\omega_x/\omega_y = 0.8$). On the BCS-side, the dashed line indicates the frequency $2\omega_y$ for the collisionless case.

modes [128]. We see that, within the experimental uncertainties, the measurements agree reasonably well with those limits (15).

For a quantitative comparison of our early compression mode measurement with theory and also with the experiments of the Duke group, the ellipticity turned out to be the main problem. However, as an unintended benefit of this experimental imperfection, the larger difference between the frequencies in the hydrodynamic and the collisionless regime strongly enhanced the visibility of the transition between these two regimes.

6·5. *Precision test of the equation of state*. – Collective modes with compression character can serve as sensitive probes to test the equation of state of a superfluid gas in the BEC-BCS crossover. The fact that a compression mode frequency is generally lower for a Fermi gas in the unitarity limit than in the mBEC case simply reflects the larger compressibility of a Fermi gas as compared to a BEC. The data provided by the experiments in Innsbruck [34] and at Duke University [33, 125] in 2004 opened up an intriguing possibility for quantitative tests of BEC-BCS crossover physics. For such precision tests, frequency measurements of collective modes are superior to the simple size measurements discussed in Sec. **5**. It is an important lesson that one learns from metrology that it is often very advantageous to convert the quantity to be measured into a frequency. In this spirit, the radial breathing mode can be seen as an excellent instrument to convert compressibility into a frequency for accurate measurements.

---

(15) The slight deviation in the unitarity limit is likely due to the anharmonicity of the trapping potential, which is not taken into account in the calculation of the frequencies.

A comparison of the axial mode data from Innsbruck and the measurements on the radial breathing mode from Duke University with mean-field BCS theory showed reasonable agreement [116, 121, 117]. This, however, was somewhat surprising as mean-field BCS theory has the obvious shortcoming that it does not account for beyond-mean-field effects [130, 131]. The latter were expected to up-shift the compression mode frequencies in the strongly interacting mBEC regime [110], but they seemed to be absent in the experiments. Advanced theoretical calculations based on a quantum Monte-Carlo approach [90] confirmed the expectation of beyond-mean-field effects in the equation of state and corresponding up-shifts in the collective mode frequencies as compared to mean-field BCS theory [121, 117].

The apparent discrepancy between theory and experiments (^{16}) motivated us to perform a new generation of collective mode experiments [71] with much higher precision and with much better control of systematic effects. To achieve a 10^{-3} accuracy level, small ellipticity and anharmonicity corrections had to be taken into account. In Fig. 18 we present our measurements on the frequency of the radial breathing mode in the BEC-BCS crossover. Because of the very low uncertainties it can be clearly seen that our data agrees with the quantum Monte-Carlo equation of state, thus ruling out mean-field BCS theory. Our experimental results also demonstrate the presence of the long-sought beyond-mean-field effects in the strongly interacting BEC regime, which shift the normalized frequency somewhat above the value of two, which one would obtain for a weakly interacting BEC.

To obtain experimental results valid for the zero-temperature limit (Fig. 18) it was crucial to optimize the timing sequence to prepare the gas in the BEC-BCS crossover with a minimum of heating after the production of the mBEC as a starting point. A comparison of the ultralow damping rates observed in our new measurements with the previous data from 2004 shows that the new experiments were indeed performed at much lower temperatures. We are convinced that temperature-induced shifts provide a plausible explanation for the earlier measurements being closer to the predictions of mean-field BCS theory than to the more advanced quantum Monte-Carlo results. For the strongly interacting mBEC regime, we indeed observed heating (presumably due to

---

(^{16}) The discrepancy between the first experiments at Duke [33] and in Innsbruck [34] disappeared when we understood the problem of ellipticity in our setup (see Sec. **6**˙4).

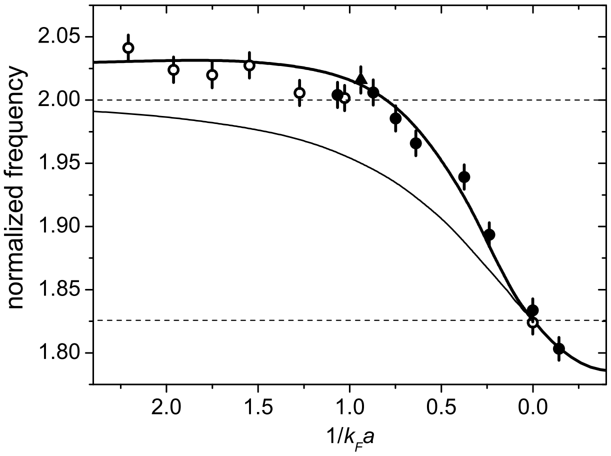

Fig. 18. – Precision measurements of the radial breathing mode frequency versus interaction parameter $1/k_{\rm F}a$ in comparison with theoretical calculations [71]. The frequency is normalized to the radial trap frequency. The experimental data include small corrections for trap ellipticity and anharmonicity and can thus be directly compared to theory in the limit of an elongated trap with cylindrical symmetry (see **6**˙1). The open and filled circles refer to measurements at trap frequencies $(\omega_{\rm x}\omega_{\rm y})^{1/2}$ of 290 Hz and 590 Hz, respectively. Here $\omega_{\rm x}/\omega_{\rm y}$ was typically between 0.91 and 0.94. The filled triangle shows a zero-temperature extrapolation of a set of measurements on the temperature dependence of the frequency. The theory curves refer to mean-field BCS theory (lower curve) and quantum Monte-Carlo calculations (upper curve) and correspond to the data presented in Ref. [117]. The horizontal dashed lines indicate the values for the BEC limit and the unitarity limit (see Table II).

inelastic processes) to cause significant down-shifts of the breathing mode frequency [71].

To put these results into a broader perspective, our precision measurements on collective modes in the BEC-BCS crossover show that ultracold Fermi gases provide a unique testing ground for advanced many-body theories for strongly interacting systems.

6˙6. *Other modes of interest.* – At the time of the Varenna Summer School we had started a set of measurements on the radial quadrupole mode in the BEC-BCS crossover [124]. This mode had not been investigated before. We implemented a two-dimensional acousto-optical scanning system for the trapping laser beam; this allows us to produce time-averaged optical potentials [132, 133], in particular potentials with variable ellipticities. With this new system, it is straightforward to create an appropriate deformation of the trapping potential to excite the quadrupole mode and other interesting modes. Here we just show the oscillation of the radial quadrupole mode for a universal Fermi gas right on resonance at $B = 834\,{\rm G}$ for the lowest temperatures that we can achieve (Fig. 19). The mode indeed exhibits the expected frequency ($\omega_{\rm q} = \sqrt{2}\,\omega_{\rm r}$), which nicely demonstrates the hydrodynamic behavior. Moreover, we find that the damping is considerably faster than for the radial compression mode at the same temperature.

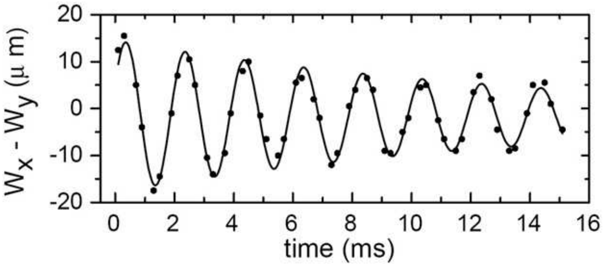

Fig. 19. – Radial quadrupole oscillation of the universal Fermi gas with unitarity-limited interactions at $B = 834\,\mathrm{G}$. We plot the difference in horizontal and vertical widths after a free expansion time of 2 ms as a function of the variable hold time in the trap. The measured oscillation frequency $\omega_\mathrm{q}/2\pi = 499\,\mathrm{Hz}$ exactly corresponds to $\sqrt{2}\,\omega_\mathrm{r}$.

Scissors modes [134, 108, 135, 136] represent another interesting class of collective excitations which we can investigate with our new system. A scissors mode is excited by a sudden rotation of an elliptic trapping potential. Scissors modes may serve as a new tool to study the temperature dependence of hydrodynamics in the BEC-BCS crossover. Scissors modes are closely related to rotations [137] and may thus provide additional insight into the collisional or superfluid nature of hydrodynamics.

7. – Pairing-gap spectroscopy in the BEC-BCS crossover

In the preceding sections we have discussed our experiments on important *macroscopic* properties of the strongly interacting Fermi gas, like potential energy, hydrodynamics, and the equation of state. We will now present our experimental results on the observation of the "pairing gap" [35], which is a *microscopic* property essential in the context of superfluidity. The gap shows the pairing energy and thus characterizes the nature of pairing in the crossover; see discussion in **5**˙1.

Historically, the observation of a pairing gap marked an important experimental breakthrough in research on superconductivity in the 1950s [138, 139, 80]. The gap measurements provided a key to investigating the paired nature of the particles responsible for the frictionless current in metals at very low temperatures. The ground-breaking BCS theory [79, 80], developed at about the same time, showed that two electrons in the degenerate Fermi sea can be coupled by an effectively attractive interaction and form a delocalized, composite particle with bosonic character. BCS theory predicted that the gap in the low-temperature limit is proportional to the critical temperature T_c (Eq. **??**), which was in agreement with the experimental observations from gap spectroscopy.

Here we will first discuss radio-frequency spectroscopy as our method to investigate pairing in different regimes (**7**˙1). We will then show how molecular pairing can be investigated and precise data on the binding energy can be obtained (**7**˙2). Finally, we will discuss our results on pairing in the many-body regimes of the crossover (**7**˙3), including the temperature dependence of the gap.

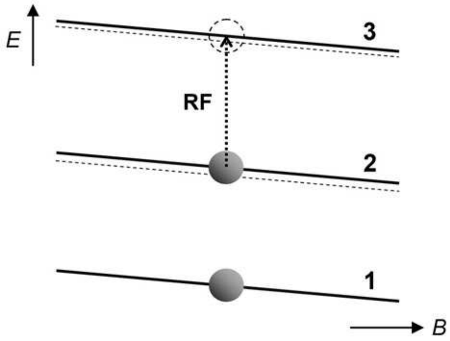

Fig. 20. – Illustration of the basic principle of RF spectroscopy for ^{6}Li at high-magnetic fields (see also Fig. 1). The three states 1, 2, and 3 essentially differ by the orientation of the nuclear spin (m_I = 1, 0, -1, respectively). By driving RF transitions the spins can be flipped and atoms are transferred from state 2 to the empty state 3. In the region of the broad Feshbach resonance, the splitting between the RF coupled states 2 and 3 is about 82 MHz. The RF does not couple states 1 and 2 because of their smaller splitting of about 76 MHz. In the mean-field regime, interactions result in effective level shifts (dashed lines).

7˙1. *Basics of radio-frequency spectroscopy.* – Radio-frequency (RF) spectroscopy has proven a powerful tool for investigating interactions in ultracold Fermi gases. In 2003, the method was introduced by the JILA group for ^{40}K [140, 23] and by the MIT group for ^{6}Li [141].

The basic idea of RF spectroscopy can be easily understood by looking on the simple Zeeman diagram of ^{6}Li in the high-field region; see also section **3**˙1 for a more detailed discussion of the energy levels. The ^{6}Li spin mixture populates states 1 and 2 (magnetic quantum numbers $m_I = 1, 0$), whereas state 3 ($m_I = -1$) is empty. RF-induced transitions can transfer atoms from state 2 to the empty state 3. The experimental signature in a state-selective detection scheme (e.g. absorption imaging) is the appearance of particles in state 3 or the disappearance of particles in state 2 (^{17}).

In the non-interacting case, the transition frequency is determined by the magnetic field through the well-known Breit-Rabi formula. We found that interactions are in general very small for "high" temperatures of a few T_F. We perform such measurements for the calibration of the magnetic field used for interaction tuning. In the experiment, the transition frequency can be determined within an uncertainty of ~100 Hz, which corresponds to magnetic field uncertainties as low as a ~20 mG.

In the mean-field regime of a weakly interacting Fermi gas, interactions lead to a shift

---

(^{17}) In a dense gas of ^{6}Li, atoms in state 3 show a very rapid decay, which we attribute to three-body collisions with 1 and 2. With atoms in three different spin states, a three-body recombination event is not Pauli suppressed and therefore very fast. This is the reason why all our measurements show the loss from state 2 instead of atoms appearing in 3.

of the RF transition frequency [140] given by $\Delta\nu_{\rm mf} = 2\hbar m^{-1}\, n_1(a' - a)$, where $n_1 = n/2$ is the number density of atoms in state 1 and a' is the scattering length for interactions between atoms in 1 and 3. In experimental work on ^{40}K [140], this mean-field shift was used to measure the change of the scattering length a near a Feshbach resonance under conditions where a' just gives a constant, non-resonant offset value. In ^{6}Li the interpretation of the differential mean-field shift is somewhat more complicated because both scattering length a and a' show resonant behavior [141, 45].

In the strongly interacting regime, the MIT group made the striking observation of the absence of interaction shifts [141]. This experimental finding, which is also of great relevance for the interpretation of our results on RF spectroscopy in the crossover (see **7**.3), is related to the fact that for ^{6}Li both a and a' are very large. In this case all resonant interactions are unitarity-limited, so that differential interaction shifts are absent.

Regarding the sensitivity of RF spectroscopy to small interaction effects, which typically occur on the kHz scale or even below, ^{6}Li features an important practical advantage over ^{40}K. In the relevant magnetic-field region around 834 G the ^{6}Li RF-transition frequency changes by -5.6 kHz/G, in contrast to 170 kHz/G near the 202 G Feshbach resonance used in the crossover experiments in ^{40}K. This large difference results from decoupling of the nuclear spin from the electron spin in ^{6}Li at high magnetic fields. The fact that a strongly interacting Fermi gas of ^{6}Li is about 30 times less susceptible to magnetic field imperfections, like fluctuations, drifts, and inhomogeneities, facilitates precise measurements of small interaction effects.

7.2. *Rf spectroscopy on weakly bound molecules.* – The application of RF spectroscopy to measure binding energies of ultracold molecules was introduced by the JILA group in Ref. [23]. We have applied RF spectroscopy to precisely determine the molecular energy structure of ^{6}Li, which also yields precise knowledge of the two-body scattering properties [45]. Meanwhile, RF spectroscopy has found various applications to ultracold Feshbach molecules [142, 143, 144, 145].

The basic idea of RF spectroscopy applied to weakly bound molecules is illustrated on the left-hand side of Fig. 21. Transferring an atom from state 2 to state 3 breaks up the dimer. The RF photon with energy $h\nu_{\rm RF}$ has to provide at least the molecular binding energy $E_{\rm b}$ in addition to the bare transition energy $h\nu_{23}$. Therefore, the dissociation sets in sharply at a threshold $\nu_{23} + E_{\rm b}/h$. Above this threshold, the RF couples molecules to atom pairs in the continuum with a kinetic energy $E_{\rm kin} = E - E_{\rm b}$, where $E = h(\nu_{\rm RF} - \nu_{23})$.

The dissociation lineshape can be understood in terms of the wavefunction overlap of the molecular state with the continuum. For weakly bound dimers, where $E_{\rm b} = \hbar/(ma^2)$ (Eq. 2), this lineshape is described by [146]

$$f(E) \propto E^{-2}(E - E_{\rm b})^{1/2}(E - E_{\rm b} + E')^{-1}\,, \tag{20}$$

where $E' = \hbar/(ma'^2)$ is an energy associated with the (positive or negative) scattering length a' between states 1 and 3. The energy E' becomes important when a' is comparable to a, i.e. when both scattering channels show resonant behavior. This is the

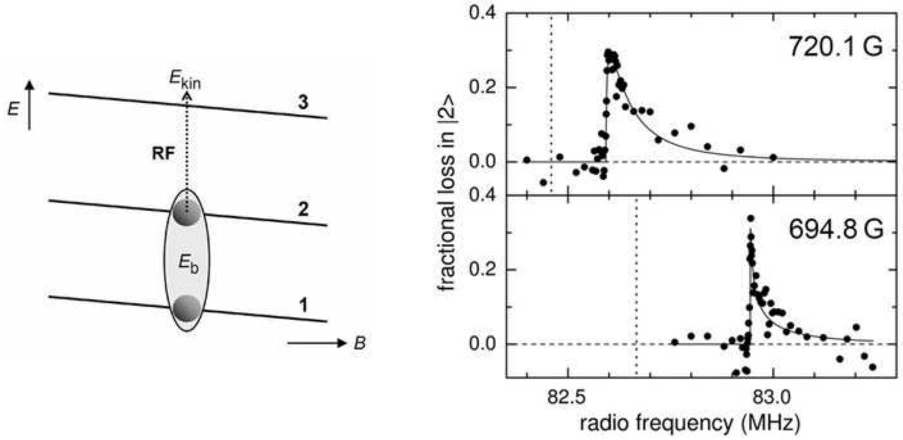

Fig. 21. – Radio-frequency spectroscopy in the molecular regime: basic principle (left-hand side) and experimental results for ^{6}Li [45] (right-hand side). To dissociate a molecule, the RF photon with energy $h\nu$ has to provide at least the molecular binding energy E_b in addition to the bare transition energy $h\nu_0$. In the experimental spectra, the onset of dissociation thus occurs shifted from the bare atomic transition frequencies, which for the two different magnetic fields are indicated by the dashed vertical lines. The solid curves show fits by the theoretical dissociation lineshapes according to Eq. 20.

case for ^{6}Li [141, 45], but not for ^{40}K [23]. In Fig. 21 (right-hand side) we show two RF-dissociation spectra taken at different magnetic fields [45]. The spectra show both the change of the binding energy E_b and the variation of the lineshape (parameter E') with the magnetic field. The experimental data is well fit by the theoretical lineshapes of Eq. 20.

To precisely determine the scattering properties of ^{6}Li [45], we used measurements of the binding energy E_b in the (1,2) channel obtained through RF-induced dissociation spectroscopy described above. In addition, we also identified bound-bound molecular transitions at magnetic fields where the channel (1,3) also supports a weakly bound molecular level ($a' > 0$). These transitions do not involve continuum states and are thus much narrower than the broad dissociation spectra. This fact facilitated very precise measurements of magnetic field dependent molecular transition frequencies. The combined spectroscopic data from bound-free and bound-bound transitions provided the necessary input to adjust the calculations based on a multi-channel quantum scattering model by our collaborators at NIST. This led to a precise characterization of the two-body scattering properties of ^{6}Li in all combinations of the loweset three spin states. This included the broad Feshbach resonance in the (1,2) channel at 834 G (see discussion in **3**˙2) and further broad resonances in the channels (1,3) and (2,3) at 690 G and 811 G, respectively.

7˙3. *Observation of the pairing gap in the crossover*. – After having discussed the application of RF spectroscopy to ultracold molecules in the preceding section, we now turn our attention to pairing in the many-body regime of the BEC-BCS crossover. The basic idea remains the same: Breaking pairs costs energy, which leads to corresponding shifts in the RF spectra. We now discuss our results of Ref. [35], where we have observed the "pairing gap" in a strongly interacting Fermi gas. Spectral signatures of pairing have been theoretically considered in Refs. [147, 148, 149, 150, 151, 152]. A clear signature of the pairing process is the emergence of a *double-peak structure* in the spectral response as a result of the coexistence of unpaired and paired atoms. The pair-related peak is located at a higher frequency than the unpaired-atoms signal.

The important experimental parameters are temperature, Fermi energy, and interaction strength. The temperature T can be controlled by variation of the final laser power of the evaporation ramp. Lacking a reliable method to determine the temperature T of a deeply degenerate, strongly interacting Fermi gas in a direct way, we measured the temperature T' after an isentropic conversion into the BEC limit. Note that, for a deeply degenerate Fermi gas, the true temperature T is substantially below our temperature parameter T' [98, 100]. The Fermi energy E_F can be controlled after the cooling process by an adiabatic recompression of the gas. The interaction strength is varied, as in our experiments described before, by slowly changing the magnetic field to the desired final value.

We recorded the RF spectra shown in Fig. 22 for different temperatures and in various coupling regimes. We studied the molecular regime at $B = 720\,\mathrm{G}$ ($a = +2170\,a_0$). For the resonance region, we examined two different magnetic fields $822\,\mathrm{G}$ ($+33,000\,a_0$) and $837\,\mathrm{G}$ ($-150,000\,a_0$), because the exact resonance location ($834.1 \pm 1.5\,\mathrm{G}$, see **3**˙2) was not exactly known at the time of our pairing gap experiments. We also studied the regime beyond the resonance with large negative scattering length at $B = 875\,\mathrm{G}$ ($a \approx -12,000\,a_0$). Spectra taken in a "hot" thermal sample at $T \approx 6T_\mathrm{F}$ ($T_\mathrm{F} = 15\mu\mathrm{K}$) show the narrow atomic $2 \to 3$ transition line (upper row in Fig. 22) and serve as a frequency reference. We present our spectra as a function of the RF offset with respect to the bare atomic transition frequency.

To understand the spectra both the homogeneous lineshape of the pair signal [148] and the inhomogeneous line broadening due to the density distribution in the harmonic trap need to be taken into account [150]. As an effect of inhomogeneity, fermionic pairing due to many-body effects takes place predominantly in the central high-density region of the trap, and unpaired atoms mostly populate the outer region of the trap where the density is low [95, 150, 101]. The spectral component corresponding to the pairs shows a large inhomogeneous broadening in addition to the homogeneous width of the pair-breaking signal. For the unpaired atoms the homogeneous line is narrow and the effects of inhomogeneity and mean-field shifts are negligible. These arguments explain why the RF spectra in general show a relatively sharp peak for the unpaired atoms together with a broader peak attributed to paired atoms.

We observed a clear double-peak structure at $T'/T_\mathrm{F} = 0.5$ (middle row in Fig. 22, $T_\mathrm{F} = 3.4\mu\mathrm{K}$). In the molecular regime (720 G), the sharp atomic peak was well separated

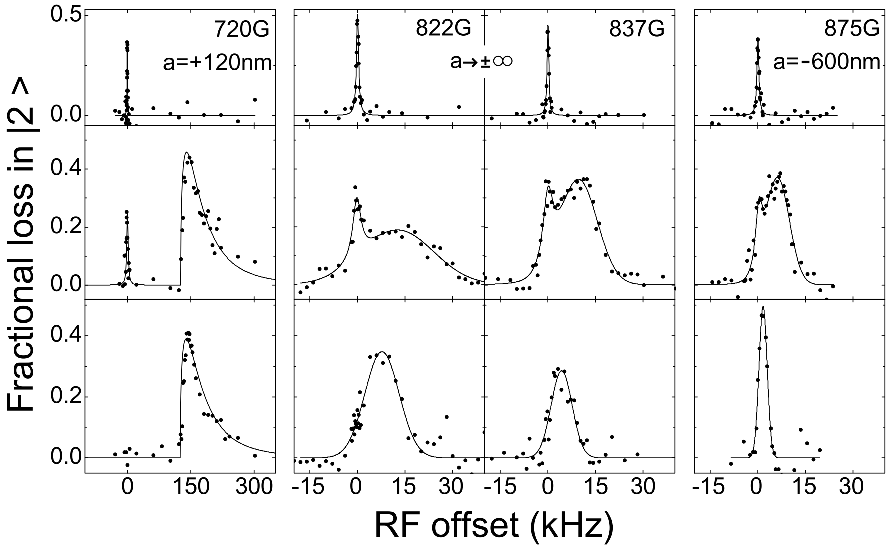

Fig. 22. – RF spectra for various magnetic fields and different degrees of evaporative cooling. The RF offset ($k_\mathrm{B} \times 1\,\mu\mathrm{K} \simeq h \times 20.8\,\mathrm{kHz}$) is given relative to the atomic transition $2 \to 3$. The molecular limit is realized for $B = 720\,\mathrm{G}$ (first column). The resonance regime is studied for $B = 822\,\mathrm{G}$ and $837\,\mathrm{G}$ (second and third column). The data at $875\,\mathrm{G}$ (fourth column) explore the crossover on the BCS side. Upper row, signals of unpaired atoms at $T' \approx 6T_\mathrm{F}$ ($T_\mathrm{F} = 15\,\mu\mathrm{K}$); middle row, signals for a mixture of unpaired and paired atoms at $T' = 0.5T_\mathrm{F}$ ($T_\mathrm{F} = 3.4\,\mu\mathrm{K}$); lower row, signals for paired atoms at $T' < 0.2T_\mathrm{F}$ ($T_\mathrm{F} = 1.2\,\mu\mathrm{K}$). Note that the true temperature T of the atomic Fermi gas is below the temperature T' which we measure in the BEC limit (see text). The solid lines are introduced to guide the eye.

from the broad dissociation signal; see discussion in **7**˙2. As the scattering length was tuned to resonance, the peaks began to overlap. In the resonance region (822 and 837 G), we still observed a relatively narrow atomic peak at the original position together with a pair signal. For magnetic fields beyond the resonance, we could resolve the double-peak structure for fields up to ~900 G.

For $T'/T_\mathrm{F} < 0.2$, we observed a disappearance of the narrow atomic peak in the RF spectra (lower row in Fig. 22, $T_\mathrm{F} = 1.2\mu\mathrm{K}$). This showed that essentially all atoms were paired. In the BEC regime (720 G) the dissociation lineshape is identical to the one observed in the trap at higher temperature and Fermi energy. Here the localized pairs are molecules with a size much smaller than the mean interparticle spacing, and the dissociation signal is independent of the density. In the resonance region (822 and 837 G) the pairing signal showed a clear dependence on the density, which became even more pronounced beyond the resonance (875 G).

To quantitatively investigate the crossover from the two-body molecular regime to the fermionic many-body regime we measured the pairing energy in a range between 720 G

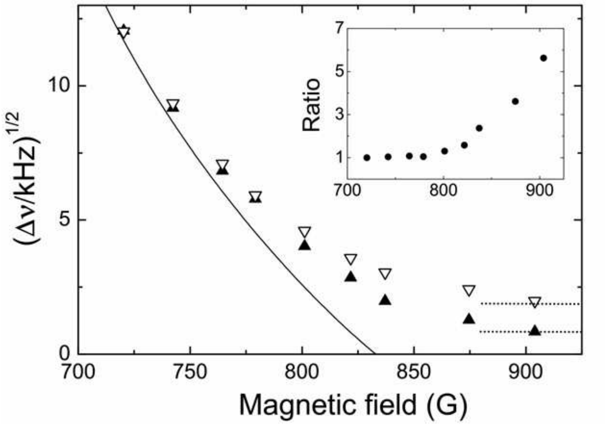

Fig. 23. – Measurements of the effective pairing gap $\Delta\nu$ as a function of the magnetic field B for deep evaporative cooling and two different Fermi temperatures $T_{\mathrm{F}} = 1.2\mu\mathrm{K}$ (filled symbols) and $3.6\mu\mathrm{K}$ (open symbols). The solid line shows $\Delta\nu$ for the low-density limit, where it is essentially given by the molecular binding energy [153]. The two dotted lines at higher magnetic fields correspond to the condition $2\Delta\nu = \omega_{\mathrm{c}}$ for the coupling of the compression mode (**6**·4) to the gap at our two different trap settings. The inset displays the ratio of the effective pairing gaps measured at the two different Fermi energies.

and 905 G. The experiments were performed after deep evaporative cooling ($T'/T_{\mathrm{F}} < 0.2$) for two different Fermi temperatures $T_{\mathrm{F}} = 1.2\,\mu\mathrm{K}$ and $3.6\,\mu\mathrm{K}$ (Fig. 23). As an *effective pairing gap* we define $\Delta\nu$ as the frequency difference between the pair-signal maximum and the bare atomic resonance. In the BEC limit, the effective pairing gap $\Delta\nu$ simply reflects the molecular binding energy E_{b}, as shown by the solid line in Fig. 23 (^{18}). With increasing magnetic field, in the BEC-BCS crossover, $\Delta\nu$ showed an increasing deviation from this low-density molecular limit and smoothly evolved into a density-dependent many-body regime where $h\Delta\nu < E_{\mathrm{F}}$.

A comparison of the pairing energies at the two different Fermi energies (inset in Fig. 23) provides further insight into the nature of the pairs. In the BEC limit, $\Delta\nu$ is solely determined by E_{b} and thus does not depend on E_{F}. In the universal regime on resonance, E_{F} is the only energy scale and we indeed observed the effective pairing gap $\Delta\nu$ to increase linearly with the Fermi energy (see Ref. [127] for more details). We found a corresponding relation $h\Delta\nu \approx 0.2\,E_{\mathrm{F}}$ (^{19}). Beyond the resonance, where the

---

(^{18}) The maximum of the dissociation signal, which defines $h\Delta\nu$ in the molecular regime, varies between E_{B} and $(4/3)\,E_{\mathrm{B}}$, depending on E'/E_{b} in Eq. 20. The solid line takes this small variation into account [153].

(^{19}) Note that there is a quantitative deviation between this experimental result for the unitarity limit (see also [127]) and theoretical spectra [150, 151, 152], which suggest $h\Delta\nu \approx 0.35\,E_{\mathrm{F}}$. This discrepancy is still an open question. We speculate that interactions between atoms in state 1

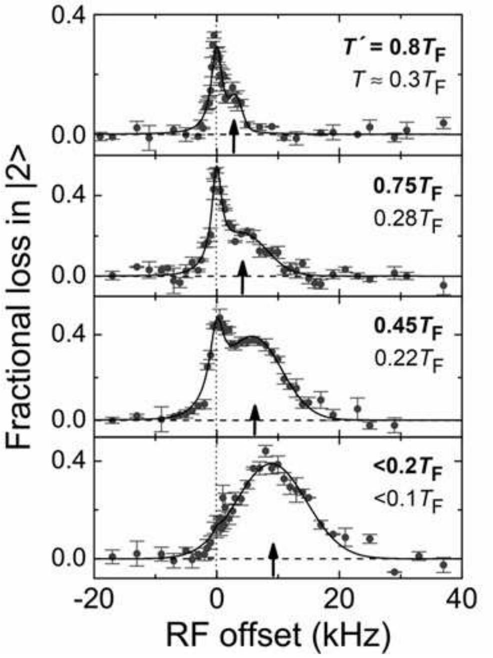

Fig. 24. – RF spectra measured at $B = 837\,\mathrm{G}$, i.e. very close to the unitarity limit, for different temperatures ($T_\mathrm{F} = 2.5\,\mu\mathrm{K}$). The temperature parameter T' was determined by measurements in the mBEC regime after an isentropic conversion of the gas. Based on the entropy calculations of Ref. [100] we also provide estimates for the true temperature T. The solid lines are fits to guide the eye using a Lorentzian curve for the atom peak and a Gaussian curve for the pair signal. The vertical dotted line marks the atomic transition and the arrows indicate the effective pairing gap $\Delta\nu$.

system is expected to change from a resonant to a BCS-type behavior, $\Delta\nu$ is found to depend more strongly on the Fermi energy and the observed gap ratio further increases. We interpret this in terms of the increasing BCS character of pairing, for which an exponential dependence $h\Delta\nu/E_\mathrm{F} \propto \exp(-\pi/2k_\mathrm{F}|a|)$ (see Table I) is expected.

In another series of measurements (Fig. 24), we applied a controlled heating method to study the temperature dependence of the gap in a way which allowed us to keep all other parameters constant. After production of a pure molecular BEC ($T' < 0.2T_\mathrm{F}$) in the usual way, we adiabatically changed the conditions to $B = 837\,\mathrm{G}$ and $T_\mathrm{F} = 1.2\,\mu\mathrm{K}$. We then increased the trap laser power by a factor of nine (T_F increased to $2.5\mu\mathrm{K}$) using exponential ramps of different durations. For fast ramps this recompression is non-adiabatic and increases the entropy. By variation of the ramp time, we explore a

---

and 3 may be responsible for this, which have not been fully accounted for in theory.

range from our lowest temperatures up to $T'/T_{\rm F} = 0.8$. The emergence of the gap with decreasing temperature is clearly visible in the RF spectra (Fig. 24). The marked increase of $\Delta\nu$ for decreasing temperature is in good agreement with theoretical expectations for the pairing gap energy [81].

Our pairing gap experiments were theoretically analyzed in Refs. [150, 151, 152]. The calculated RF spectra are in agreement with our experimental results and demonstrate how a double-peak structure emerges as the gas is cooled below $T/T_{\rm F} \approx 0.5$ and how the atomic peak disappears with further decreasing temperature. In particular, the theoretical work clarifies the role of the pseudo-gap regime [81, 99] in our experiments, where pairs are formed before superfluidity is reached. We believe that, the upper spectrum of Fig. 24 ($T' = 0.8\,T_{\rm F}$, corresponding to $T = 0.3\,T_{\rm F}$ [100]) shows the pseudo-gap regime. The lower spectrum, however, which was taken at a much lower temperature ($T' < 0.2\,T_{\rm F}$, $T < 0.1\,T_{\rm F}$), is deep in the superfluid regime. Here, the nearly complete disappearance of the atom peak shows that fermionic pairing took place even in the outer region of the trapped gas where the density and the local Fermi energy are low. According to theory [150, 151] this happens well below the critical temperature for the formation of a resonance superfluid in the center of the trap. This conclusion [35] fits well to the other early observations that suggested superfluidity in experiments performed under similar conditions [33, 34], and also to the observation of superfluidity by vortex formation in Ref. [38].

We finally point to an interesting connection to our measurements on radial collective excitations (**6**˙4), where an abrupt breakdown of hydrodynamics was observed at a magnetic field of about 910 G [34]. The hydrodynamic equations which describe collective excitations implicitly assume a large gap, and their application becomes questionable when the gap is comparable to the radial oscillation frequency [154]. We suggest a pair breaking condition $\omega_{\rm c} = 2h\Delta\nu$ (^{20}), which roughly corresponds to $\omega_{\rm r} = h\Delta\nu$ ($\omega_{\rm c} \approx 2\omega_{\rm r}$). Our pair breaking condition is illustrated by the dashed lines in Fig. 23 for the two different Fermi energies of the experiment. In both cases the effective gap $\Delta\nu$ reaches the pair breaking condition somewhere slightly above 900 G. This is in striking agreement with our observations on collective excitations at various Fermi temperatures [34, 127]. This supports the explanation that pair breaking through coupling of oscillations to the gap leads to strong heating and large damping and thus to a breakdown of superfluidity on the BCS side of the resonance.

8. – Conclusion and outlook

Ultracold Fermi gases represent one of the most exciting fields in present-day physics. Here experimental methods of atomic, molecular, and optical physics offer unprecedented possibilities to explore fundamental questions related to many different fields of physics.

(^{20}) The factor of 2 in this condition results from the fact that here pair breaking creates two in-gap excitations, instead of one in-gap excitation in the case of RF spectroscopy, where one particle is removed by transfer into an empty state.

In the last few years, we have seen dramatic and also surprising developments, which have already substantially improved our understanding of the interaction properties of fermions. Amazing progress has been achieved in the exploration of the crossover of strongly interacting system from BEC-type to BCS-type behavior. Resonance superfluidity now is well established. Recent experimental achievements have made detailed precision tests of advanced many-body quantum theories possible.

The majority of experiments have so far been focused on bulk systems of two-component spin mixtures in macroscopic traps; however, ultracold gases offer many more possibilities to realized intriguing new situations. The recent experiments on imbalanced systems [39, 40] give us a first impression how rich the physics of fermionic systems will be when more degrees of freedom will be present. As another important example, optical lattices [155, 8, 156] allows us to model the periodic environment of crystalline materials, providing experimental access to many interesting questions in condensed-matter physics [157]. Also, fermionic mixtures of different atomic species open up many new possibilities. In Bose-Fermi mixtures [158, 159, 160, 145], fermionic pairing and superfluidity can be mediated through a bosonic background [161, 162]. In the case of Fermi-Fermi mixtures [163], pairing between particles of different masses [164] and novel regimes of superfluidity represent intriguing prospects for future research.

With the recent experiments on the physics of ultracold fermions, we have just opened the door to an exciting new research field. On the large and widely unexplored terrain, many new challenges (and surprises) are surely waiting for us!

* * *

Our work on ultracold Fermi gases, which developed in such an exciting way, is the result of a tremendous team effort over the past eight years. Its origin dates back to my former life in Heidelberg (Germany), where our activities on ultracold fermions began in the late 1990s. I thank the team of these early days (A. Mosk, M. Weidemüller, H. Moritz, T. Elsässer) for the pioneering work to start our adventures with ^{6}Li. The experiment moved to Innsbruck in 2001, and many people have contributed to its success there. For their great work and achievements, I thank the Ph.D. students S. Jochim (who moved with the experiment from Heidelberg to Innsbruck) and M. Bartenstein, A. Altmeyer, and S. Riedl, along with the diploma students G. Hendl and C. Kohstall. Also, I acknowledge the important contributions by the post-docs R. Geursen and M. Wright (thanks, Matt, also for the many useful comments on the manuscript). I am greatly indebted to C. Chin, who shared a very exciting time with us and stimulated the experiment with many great ideas, and my long-standing colleague J. Hecker Denschlag for their invaluable contributions. The experiment strongly benefited from the great synergy in a larger group (`www.ultracold.at`) and from the outstanding scientific environment in Innsbruck. Finally, I thank the Austrian Science Fund FWF for funding the experiment through various programs, and the European Union for support within the Research Training Network “Cold Molecules”.

REFERENCES

[1] DeMarco B. and Jin D.S. *Science*, **285** (1999) 1703.

[2] Truscott A.G., Strecker K.E., McAlexander W.I., Partridge G.B. and Hulet R.G. *Science*, **291** (2001) 2570.

[3] Schreck F., Khaykovich L., Corwin K.L., Ferrari G., Bourdel T., Cubizolles J. and Salomon C. *Phys. Rev. Lett.*, **87** (2001) 080403.

[4] Granade S.R., Gehm M.E., O'Hara K.M. and Thomas J.E. *Phys. Rev. Lett.*, **88** (2002) 120405.

[5] Hadzibabic Z., Stan C.A., Dieckmann K., Gupta S., Zwierlein M.W., Görlitz A. and Ketterle W. *Phys. Rev. Lett.*, **88** (2002) 160401.

[6] Roati G., Riboli F., Modugno G. and Inguscio M. *Phys. Rev. Lett.*, **89** (2002) 150403.

[7] Jochim S., Bartenstein M., Altmeyer A., Hendl G., Riedl S., Chin C., Hecker Denschlag J. and Grimm R. *Science*, **302** (2003) 2101.

[8] Köhl M., Moritz H., Stöferle T., Günter K. and Esslinger T. *Phys. Rev. Lett.*, **94** (2005) 080403.

[9] Silber C., Gunther S., Marzok C., Deh B., Courteille P.W. and Zimmermann C. *Phys. Rev. Lett.*, **95** (2005) 170408.

[10] Ospelkaus C., Ospelkaus S., Sengstock K. and Bongs K. *Phys. Rev. Lett.*, **96** (2006) 020401.

[11] Aubin S., Myrskog S., Extavour M.H.T., Leblanc L.J., Mckay D., Stummer A. and Thywissen J.H. *Nature Phys.*, **2** (2006) 384.

[12] McNamara J.M., Jeltes T., Tychkov A.S., Hogervorst W. and Vassen W. *Phys. Rev. Lett.*, **97** (2006).

[13] Fukuhara T., student talk presented at the School; see also cond-mat/0607228.

[14] *Bose-Einstein Condensation in Atomic Gases*, Proceedings of the International School of Physics "Enrico Fermi", Course CXL, Varenna, 7-17 July 1998, edited by M. Inguscio, S. Stringari and C. E. Wieman.

[15] Tiesinga E., Verhaar B.J. and Stoof H.T.C. *Phys. Rev. A*, **47** (1993) 4114.

[16] Inouye S., Andrews M.R., Stenger J., Miesner H.J., Stamper-Kurn D.M. and Ketterle W. *Nature*, **392** (1998) 151.

[17] Roberts J.L., Claussen N.R., Cornish S.L. and Wieman C.E. *Phys. Rev. Lett.*, **85** (2000) 728.

[18] Weber T., Herbig J., Mark M., Nagerl H.C. and Grimm R. *Phys. Rev. Lett.*, **91** (2003) 123201.

[19] Kraemer T., Mark M., Waldburger P., Danzl J.G., Chin C., Engeser B., Lange A.D., Pilch K., Jaakkola A., Nägerl H.C. and Grimm R. *Nature*, **440** (2006) 315.

[20] Greiner M., Mandel O., Esslinger T., Hänsch T.W. and Bloch I. *Nature*, **415** (2002) 39.

[21] O'Hara K.M., Hemmer S.L., Gehm M.E., Granade S.R. and Thomas J.E. *Science*, **298** (2002) 2179.

[22] Bourdel T., Cubizolles J., Khaykovich L., Magalhães K.M.F., Kokkelmans S.J.J.M.F., Shlyapnikov G.V. and Salomon C. *Phys. Rev. Lett.*, **91** (2003) 020402.

[23] Regal C.A., Ticknor C., Bohn J.L. and Jin D.S. *Nature*, **424** (2003) 47.

[24] Strecker K.E., Partridge G.B. and Hulet R.G. *Phys. Rev. Lett.*, **91** (2003) 080406.

[25] Cubizolles J., Bourdel T., Kokkelmans S.J.J.M.F., Shlyapnikov G.V. and Salomon C. *Phys. Rev. Lett.*, **91** (2003) 240401.

[26] Jochim S., Bartenstein M., Altmeyer A., Hendl G., Chin C., Hecker Denschlag J. and Grimm R. *Phys. Rev. Lett*, **91** (2003) 240402.

[27] Greiner M., Regal C.A. and Jin D.S. *Nature*, **426** (2003) 537.

[28] Zwierlein M.W., Stan C.A., Schunck C.H., Raupach S.M.F., Gupta S., Hadzibabic Z. and Ketterle W. *Phys. Rev. Lett.*, **91** (2003) 250401.

[29] Bourdel T., Khaykovich L., Cubizolles J., Zhang J., Chevy F., Teichmann M., Tarruell L., Kokkelmans S.J.J.M.F. and Salomon C. *Phys. Rev. Lett.*, **93** (2004) 050401.

[30] Regal C.A., Greiner M. and Jin D.S. *Phys. Rev. Lett.*, **92** (2004) 040403.

[31] Zwierlein M.W., Stan C.A., Schunck C.H., Raupach S.M.F., Kerman A.J. and Ketterle W. *Phys. Rev. Lett.*, **92** (2004) 120403.

[32] Bartenstein M., Altmeyer A., Riedl S., Jochim S., Chin C., Hecker Denschlag J. and Grimm R. *Phys. Rev. Lett.*, **92** (2004) 120401.

[33] Kinast J., Hemmer S.L., Gehm M.E., Turlapov A. and Thomas J.E. *Phys. Rev. Lett.*, **92** (2004) 150402.

[34] Bartenstein M., Altmeyer A., Riedl S., Jochim S., Chin C., Hecker Denschlag J. and Grimm R. *Phys. Rev. Lett.*, **92** (2004) 203201.

[35] Chin C., Bartenstein M., Altmeyer A., Riedl S., Jochim S., Hecker Denschlag J. and Grimm R. *Science*, **305** (2004) 1128.

[36] Partridge G.B., Strecker K.E., Kamar R.I., Jack M.W. and Hulet R.G. *Phys. Rev. Lett.*, **95** (2005) 020404.

[37] Kinast J., Turlapov A., Thomas J.E., Chen Q., Stajic J. and Levin K. *Science*, **307** (2005) 1296.

[38] Zwierlein M.W., Abo-Shaeer J.R., Schirotzek A., Schunck C.H. and Ketterle W. *Nature*, **435** (2005) 1047.

[39] Partridge G.B., Li W., Kamar R.I., Liao Y. and Hulet R.G. *Science*, **311** (2005) 503.

[40] Zwierlein M.W., Schirotzek A., Schunck C.H. and Ketterle W. *Science*, **311** (2005) 492.

[41] Zwierlein M.W., Schirotzek A., Schunck C.H. and Ketterle W. *Nature*, **442** (2006) 54.

[42] Loftus T., Regal C.A., Ticknor C., Bohn J.L. and Jin D.S. *Phys. Rev. Lett.*, **88** (2002) 173201.

[43] Arimondo E., Inguscio M. and Violino P. *Rev. Mod. Phys.*, **49** (1977) 31.

[44] Houbiers M., Stoof H.T.C., McAlexander W.I. and Hulet R.G. *Phys. Rev. A*, **57** (1998) R1497.

[45] Bartenstein M., Altmeyer A., Riedl S., Geursen R., Jochim S., Chin C., Hecker Denschlag J., Grimm R., Simoni A., Tiesinga E., Williams C.J. and Julienne P.S. *Phys. Rev. Lett.*, **94** (2005) 103201.

[46] Abraham E.R.I., McAlexander W.I., Gerton J.M., Hulet R.G., Côté R. and Dalgarno A. *Phys. Rev. A*, **55** (1997) R3299.

[47] Dieckmann K., Stan C.A., Gupta S., Hadzibabic Z., Schunck C.H. and Ketterle W. *Phys. Rev. Lett.*, **89** (2002) 203201.

[48] OHara K.M., Hemmer S.L., Granade S.R., Gehm M.E., Thomas J.E., Venturi V., Tiesinga E. and Williams C.J. *Phys. Rev. A*, **66** (2002) 041401.

[49] Jochim S., Bartenstein M., Hendl G., Hecker Denschlag J., Grimm R., Mosk A. and Weidemüller W. *Phys. Rev. Lett*, **89** (2002) 273202.

[50] Jochim S. *Bose-Einstein Condensation of Molecules*. Ph.D. thesis, Innsbruck University (2004).

[51] Schunck C.H., Zwierlein M.W., Stan C.A., Raupach S.M.F. and Ketterle W. *Phys. Rev. A*, **71** (2005) 045601.

[52] Zhang J., van Kempen E.G.M., Bourdel T., Khaykovich L., Cubizolles J., Chevy F., Teichmann M., Taruell L., Kokkelmans S.J.J.M.F. and Salomon C. *Phys. Rev. A*, **70** (2004) 030702(R).

[53] Gribakin G.F. and Flambaum V.V. *Phys. Rev. A*, **48** (1993) 546.

[54] Jensen A.S., Riisager K., Fedorov D.V. and Garrido E. *Rev. Mod. Phys.*, **76** (2004) 215.

[55] Braaten E. and Hammer H.W. *Phys. Rep.*, **428** (2006) 259.

[56] Petrov D.S., Salomon C. and Shlyapnikov G.V. *Phys. Rev. Lett.*, **93** (2004) 090404.

[57] Donley E.A., Clausen N.R., Thompson S.T. and Wieman C.E. *Nature*, **417** (2002) 529.

[58] Herbig J., Kraemer T., Mark M., Weber T., Chin C., Nägerl H.C. and Grimm R. *Science*, **301** (2003) 1510.

[59] Dürr S., Volz T., Marte A. and Rempe G. *Phys. Rev. Lett.*, **92** (2004) 020406.

[60] Xu K., Mukaiyama T., Abo-Shaeer J.R., Chin J.K., Miller D.E. and Ketterle W. *Phys. Rev. Lett.*, **91** (2003) 210402.

[61] Regal C.A., Greiner M. and Jin D.S. *Phys. Rev. Lett.*, **92** (2004) 083201.

[62] Metcalf H.J. and van der Straten P. *Laser Cooling and Trapping* (Springer, New York, 1999).

[63] Schünemann U., Engler H., Zielonkowski M., Weidemüller M. and Grimm R. *Opt. Commun.*, **158** (1998) 263.

[64] Grimm R., Weidemüller M. and Ovchinnikov Y.B. *Adv. At. Mol. Opt. Phys.*, **42** (2000) 95.

[65] Hadzibabic Z., Gupta S., Stan C.A., Schunck C.H., Zwierlein M.W., Dieckmann K. and Ketterle W. *Phys. Rev. Lett.*, **91** (2003) 160401.

[66] Pinkse P.W.H., Mosk A., Weidemüller M., Reynolds M.W., Hijmans T.W. and Walraven J.T.M. *Phys. Rev. Lett.*, **78** (1997) 990.

[67] Stamper-Kurn D.M., Miesner H.J., Chikkatur A.P., Inouye S., Stenger J. and Ketterle W. *Phys. Rev. Lett.*, **81** (1998) 2194.

[68] Weber T., Herbig J., Mark M., Nägerl H.C. and Grimm R. *Science*, **299** (2003) 232.

[69] Rychtarik D., Engeser B., Nägerl H.C. and Grimm R. *Phys. Rev. Lett.*, **92** (2004) 173003.

[70] Mosk A., Jochim S., Elsässer T., Weidemüller M. and Grimm R. *Optics Lett.*, **26** (2001) 1837.

[71] Altmeyer A., Riedl S., Kohstall C., Wright M., Geursen R., Bartenstein M., Chin C., Denschlag J.H. and Grimm R. *cond-mat/0609390* (2006).

[72] Chin C. and Grimm R. *Phys. Rev. A*, **69** (2004) 033612.

[73] Kokkelmans S.J.J.M.F., Shlyapnikov G.V. and Salomon C. *Phys. Rev. A*, **69** (2004) 031602.

[74] Barrett M.D., Sauer J.A. and Chapman M.S. **87** (2001) 010404.

[75] Kinoshita T., Wenger T. and Weiss D.S. *Phys. Rev. A*, **71** (2005) 011602(R).

[76] Eagles D.M. *Phys. Rev.*, **186** (1969) 456.

[77] Leggett A.J. In A. Pekalski and R. Przystawa, editors, *Modern Trends in the Theory of Condensed Matter*, volume 115 of *Lecture Notes in Physics*, p. 13 (Springer Verlag, Berlin, 1980).

[78] Nozières P. and Schmitt-Rink S. *J. Low Temp. Phys.*, **59** (1985) 195.

[79] Bardeen J., Cooper L.N. and Schrieffer J.R. *Phys. Rev.*, **108** (1957) 1175.

[80] Tinkham M. *Introduction to Superconductivity* (McGraw-Hill, New York, 1996), second edition.

[81] Chen Q., Stajic J., Tan S. and Levin K. *Phys. Rep.*, **412** (2005) 1.

[82] Holland M., Kokkelmans S.J.J.M.F., Chiofalo M.L. and Walser R. *Phys. Rev. Lett.*, **87** (2001) 120406.

[83] Timmermans E., Furuya K., Milloni P.W. and Kerman A.K. *Phys. Lett. A*, **285** (2001) 228.

[84] Butts D.A. and Rokhsar D.S. *Phys. Rev. A*, **55** (1997) 4346.

[85] Baker G.A. *Phys. Rev. C*, **60** (1999) 054311.

[86] Heiselberg H. *Phys. Rev. A*, **63** (2001) 043606.

[87] Ho T.L. *Phys. Rev. Lett.*, **92** (2004) 090402.

[88] Bruun G.M. *Phys. Rev. A*, **70** (2004) 053602.

[89] Carlson J., Chang S.Y., Pandharipande V.R. and Schmidt K.E. *Phys. Rev. Lett.*, **91** (2003) 050401.

[90] Astrakharchik G.E., Boronat J., Casulleras J. and Giorgini S. *Phys. Rev. Lett.*, **93** (2004) 200404.

[91] Perali A., Pieri P. and Strinati G.C. *Phys. Rev. Lett.*, **93** (2004) 100404.

[92] Stewart J.T., Gaebler J.P., Regal C.A. and Jin D.S. *Phys. Rev. Lett.*, **97** (2006) 220406.

[93] Heiselberg H. *Phys. Rev. Lett.*, **93** (2004) 040402.

[94] Dalfovo F., Giorgini S., Pitaevskii L.P. and Stringari S. *Rev. Mod. Phys.*, **71** (1999) 463.

[95] Perali A., Pieri P., Pisani L. and Strinati G.C. *Phys. Rev. Lett.*, **92** (2004) 220404.

[96] Gor'kov L.P. and Melik-Barkhudarov T.K. *Sov. Phys. JETP*, **13** (1961) 1018.

[97] Combescot R. *Phys. Rev. Lett.*, **83** (1999) 3766.

[98] Carr L.D., Shlyapnikov G.V. and Castin Y. *Phys. Rev. Lett.*, **92** (2004) 150404.

[99] Stajic J., Milstein J.N., Chen Q., Chiofalo M.L., Holland M.J. and Levin K. *Phys. Rev. A*, **69** (2004) 063610.

[100] Chen Q., Stajic J. and Levin K. *Phys. Rev. Lett.*, **95** (2005) 260405.

[101] Stajic J., Chen Q. and Levin K. *Phys. Rev. Lett.*, **94** (2005) 060401.

[102] Jin D.S., Ensher J.R., Matthews M.R., Wieman C.E. and Cornell E.A. *Phys. Rev. Lett.*, **77** (1996) 420.

[103] Mewes M.O., Andrews M.R., van Druten N.J., Kurn D.M., Durfee D.S., Townsend C.G. and Ketterle W. *Phys. Rev. Lett.*, **77** (1996) 988.

[104] Stringari S. *Phys. Rev. Lett.*, **77** (1996) 2360.

[105] Jin D.S., Matthews M.R., Ensher J.R., Wieman C.E. and Cornell E.A. *Phys. Rev. Lett.*, **78** (1997) 764.

[106] Stamper-Kurn D.M., Miesner H.J., Inouye S., Andrews M.R. and Ketterle W. *Phys. Rev. Lett.*, **81** (1998) 500.

[107] Onofrio R., Durfee D.S., Raman C., Köhl M., Kuklewicz C.E. and Ketterle W. *Phys. Rev. Lett.*, **84** (2000) 810.

[108] Maragò O.M., Hopkins S.A., Arlt J., Hodby E., Hechenblaikner G. and Foot C.J. *Phys. Rev. Lett.*, **84** (2000) 2056.

[109] Chevy F., Bretin V., Rosenbusch P., Madison K.W. and Dalibard J. *Phys. Rev. Lett.*, **88** (2002) 250402.

[110] Stringari S. *Europhys. Lett.*, **65** (2004) 749.

[111] DeMarco B., Papp S.B. and Jin D.S. *Phys. Rev. Lett.*, **86** (2001) 5409.

[112] Ferrari G. *Phys. Rev. A*, **59** (1999) R4125.

[113] Gupta S., Hadzibabic Z., Anglin J.R. and Ketterle W. *Phys. Rev. Lett.*, **92** (2004) 100401.

[114] Vichi L. *J. Low. Temp. Phys.*, **121** (2000) 177.
[115] Vichi L. and Stringari S. *Phys. Rev. A*, **60** (1999) 4734.
[116] Hu H., Minguzzi A., Liu X.J. and Tosi M.P. *Phys. Rev. Lett.*, **93** (2004) 190403.
[117] Astrakharchik G.E., Combescot R., Leyronas X. and Stringari S. *Phys. Rev. Lett.*, **95** (2005) 030404.
[118] Kim Y.E. and Zubarev A.L. *Phys. Rev. A*, **70** (2004) 033612.
[119] Combescot R. and Leyronas X. *Europhys. Lett.*, **68** (2004) 762.
[120] Bulgac A. and Bertsch G.F. *Phys. Rev. Lett.*, **94** (2005) 070401.
[121] Manini N. and Salasnich L. *Phys. Rev. A*, **71** (2005) 033625.
[122] Silva T.N.D. and Mueller E.J. *Phys. Rev. A*, **72** (2005) 063614.
[123] Combescot R., Kagan M.Y. and Stringari S. *Phys. Rev. A*, **74** (2006) 042717.
[124] Altmeyer A., Riedl S., Kohstall C., Wright M.J., Hecker Denschlag J. and Grimm R. *in preparation*.
[125] Kinast J., Turlapov A. and Thomas J.E. *Phys. Rev. A*, **70** (2004) 051401(R).
[126] Kinast J., Turlapov A. and Thomas J.E. *Phys. Rev. Lett.*, **94** (2005) 170404.
[127] Bartenstein M. *From Molecules to Cooper Pairs: Experiments in the BEC-BCS Crossover*. Ph.D. thesis, Innsbruck University (2005).
[128] Altmeyer A., Riedl S., Kohstall C., Wright M.J., Hecker Denschlag J. and Grimm R. *cond-mat/0611285* (2006).
[129] Thomas J.E., Kinast J. and Turlapov A. *Phys. Rev. Lett.*, **95** (2005) 120402.
[130] Lee T.D. and Yang C.N. *Phys. Rev.*, **105** (1957) 1119.
[131] Lee T.D., Huang K. and Yang C.N. *Phys. Rev.*, **106** (1957) 1135.
[132] Milner V., Hanssen J.L., Campbell W.C. and Raizen M.G. *Phys. Rev. Lett.*, **86** (2001) 1514.
[133] Friedman N., Kaplan A., Carasso D. and Davidson N. *Phys. Rev. Lett.*, **86** (2001) 1518.
[134] Guéry-Odelin D. and Stringari S. *Phys. Rev. Lett.*, **83** (1999) 4452.
[135] Minguzzi A. and Tosi M.P. *Phys. Rev. A*, **63** (2001) 023609.
[136] Cozzini M., Stringari S., Bretin V., Rosenbusch P. and Dalibard J. *Phys. Rev. A*, **67** (2003) 021602(R).
[137] Cozzini M. and Stringari S. *Phys. Rev. Lett.*, **91** (2003) 070401.
[138] Biondi M.A., Garfunkel M.P. and McCoubrey A.O. *Phys. Rev.*, **101** (1956) 1427.
[139] Glover R.E. and Tinkham M. *Phys. Rev.*, **104** (1956) 844.
[140] Regal C.A. and Jin D.S. *Phys. Rev. Lett.*, **90** (2003) 230404.
[141] Gupta S., Hadzibabic Z., Zwierlein M.W., Stan C.A., Dieckmann K., Schunck C.H., van Kempen E.G.M., Verhaar B.J. and Ketterle W. *Science*, **300** (2003) 1723.
[142] Moritz H., Stöferle T., Günter K., Köhl M. and Esslinger T. *Phys. Rev. Lett.*, **94** (2005) 210401.
[143] Stöferle T., Moritz H., Günter K., Köhl M. and Esslinger T. *Phys. Rev. Lett.*, **96** (2006) 030401.
[144] Thalhammer G., Winkler K., Lang F., Schmid S., Grimm R. and Hecker Denschlag J. *Phys. Rev. Lett.*, **96** (2006) 050402.
[145] Ospelkaus C., Ospelkaus S., Humbert L., Ernst P., Sengstock K. and Bongs K. *Phys. Rev. Lett.*, **97** (2006) 120402.
[146] Chin C. and Julienne P.S. *Phys. Rev. A*, **71** (2005) 012713.
[147] Törmä P. and Zoller P. *Phys. Rev. Lett.*, **85** (2000) 487.
[148] Kinnunen J., Rodriguez M. and Törmä P. *Phys. Rev. Lett.*, **92** (2004) 230403.
[149] Büchler H.P., Zoller P. and Zwerger W. *Phys. Rev. Lett.*, **93** (2004) 080401.
[150] Kinnunen J., Rodriguez M. and Törmä P. *Science*, **305** (2004) 1131.

[151] He Y., Chen Q. and Levin K. *Phys. Rev. A*, **72** (2005) 011602.
[152] Ohashi Y. and Griffin A. *Phys. Rev. A*, **72** (2005) 063606.
[153] See supporting online material to Ref. [35].
[154] Combescot R. and Leyronas X. *Phys. Rev. Lett.*, **93** (2004) 138901.
[155] Modugno G., Ferlaino F., Heidemann R., Roati G. and Inguscio M. *Phys. Rev. A*, **68** (2003) 011601(R).
[156] Chin J.K., Miller D.E., Liu Y., Stan C., Setiawan W., Sanner C., Xu K. and Ketterle W. *Nature*, **443** (2006) 961.
[157] Lewenstein M., Sanpera A., Ahufinger V., Damski B., Sen(De) A. and Sen U. *cond-mat/0606771* (2006).
[158] Modugno G., Roati G., Riboli F., Ferlaino F., Brecha R. and Inguscio M. *Science*, **297** (2002) 2240.
[159] Stan C.A., Zwierlein M.W., Schunck C.H., Raupach S.M.F. and Ketterle W. *Phys. Rev. Lett.*, **93** (2004) 143001.
[160] Inouye S., Goldwin J., Olsen M.L., Ticknor C., Bohn J.L. and Jin D.S. *Phys. Rev. Lett.*, **93** (2004) 183201.
[161] Bijlsma M.J., Heringa B.A. and Stoof H.T.C. *Phys. Rev. A*, **61** (2000) 053601.
[162] Efremov D.V. and Viverit L. *Phys. Rev. B*, **65** (2002) 134519.
[163] A first report on the realization of a Fermi-Fermi mixture of ^{6}Li and ^{40}K in Innsbruck was presented by G. Kerner at the *Workshop on Cold Molecules, 379th Heraeus Seminar*, Bad Honnef, Germany, 29 Oct. - 2 Nov. 2006.
[164] Petrov D.S., Salomon C. and Shlyapnikov G.V. *J. Phys. B: At. Mol. Opt. Phys.*, **38** S645.